NASA CR-54149

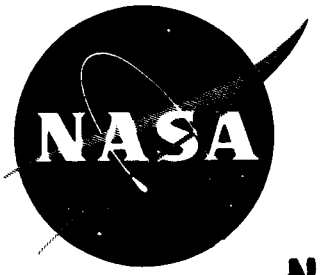

DEVELOPMENT OF A COAXIAL PLASMA GUN FOR SPACE PROPULSION

by

Terence J. Gooding, Bruce R. Hayworth,
Alan V. Larson and David E. T. F. Ashby

prepared for

NATIONAL AERONAUTICS AND SPACE ADMINISTRATION

CONTRACT NAS 3-2594

GENERAL DYNAMICS | ASTRONAUTICS
San Diego, California

NOTICE

This report was prepared as an account of Government sponsored work. Neither the United States, nor the National Aeronautics and Space Administration (NASA), nor any person acting on behalf of NASA:

A.) Makes any warranty or representation, expressed or implied, with respect to the accuracy, completeness, or usefulness of the information contained in this report, or that the use of any information, apparatus, method or process disclosed in this report may not infringe privately owned rights; or

B.) Assumes any liabilities with respect to the use of, or for damages resulting from the use of any information, apparatus, method or process disclosed in this report.

As used above, "person acting on behalf of NASA" includes any employee or contractor of NASA, or employee of such contractor, to the extent that such employee or contractor of NASA, or employee of such contractor prepares, disseminates, or provides access to, any information pursuant to his employment or contract with NASA, or his employment with such contractor.

Requests for copies of this report
should be referred to:

National Aeronautics and Space Administration
Office of Scientific and Technical Information
Washington 25, D.C.
Attention: AFSS-A

DEVELOPMENT OF A COAXIAL PLASMA GUN FOR SPACE PROPULSION

by

Terence J. Gooding, Bruce R. Hayworth,
Alan V. Larson and David E. T. F. Ashby

29222

ABSTRACT

A description is given of the work done in the third year of an experimental program to evaluate the pulsed co-axial plasma gun as a thrustor for space propulsion applications. The pursuit of efficiency has led to the development of a low loss, light weight energy storage capacitor which exhibits pulse line behavior. An energy inventory shows that the plasma resistive losses are small and that the accelerator efficiency is not limited by poor energy transfer from the energy source to the plasma. The thermal efficiency (exhaust energy/stored energy) has been increased to 45% at an average exhaust velocity of about 7 cm/μsec. A theoretical discussion shows that a significantly higher efficiency cannot be expected with the present mode of operation, but that two other modes are available which in principle have no such limitation.

auth.

54149
NAS CR-~~54149~~
GDA DBE 64-051

FINAL REPORT

DEVELOPMENT OF A COAXIAL PLASMA GUN FOR SPACE PROPULSION

by

Terence J. Gooding, Bruce R. Hayworth,
Alan V. Larson and David E. T. F. Ashby

Space Science Laboratory

prepared for

NATIONAL AERONAUTICS AND SPACE ADMINISTRATION

June 1964

CONTRACT NAS 3-2594

Project Manager
NASA Lewis Research Center
Cleveland, Ohio
Spacecraft Technology Division
Mr. Peter Ramins

GENERAL DYNAMICS/ASTRONAUTICS
San Diego, California

TABLE OF CONTENTS

LIST OF FIGURES

1.0 Introduction and Review of Previous Work

This report contains a description of the work carried out during the third year of an experimental program to evaluate the pulsed co-axial plasma gun as a thrustor for space propulsion applications. The results obtained during the first two years are presented in the final reports on the previous contracts NAS 5-1139 and NAS 3-2501.[1,2] In the following section a brief review of the program is presented together with a summary of earlier results; this is followed by sections dealing with the experimental results and the conclusions drawn from them. Three appendices are included which deal with certain theoretical aspects of co-axial accelerators, new diagnostic techniques and pulse lines respectively.

At the beginning of the program we chose to study the co-axial gun because in this device the plasma is always tightly coupled to the magnetic field, it is simple in concept and it offers the possibility of extreme reliability. The analysis of the original design was based on the model of a current sheet accelerating a constant mass of gas;[1] this model together with the requirement for high reliability and long life, led to a gun with a 1 μF capacitor. A small capacitance was thought desirable so that in a final system a vacuum dielectric could be used. During the past two years this restraint has been relaxed because of the difficulty of obtaining optimum 'matching' to the accelerator with a small capacitor, and because recent developments in energy-storage capacitors indicate that solid dielectrics should be satisfactory.

A gun with a short barrel length and a correspondingly short electrical period was chosen in order to limit the time available for the growth of instabilities at the interface between the magnetic field and the plasma; in addition it was considered that short electrodes would suffer less from

erosion than long electrodes. The gun has always been operated in the gas-triggered mode because the life-times of switches operating at high currents are much too short to consider using one in a final system.

In the first year a major effort was spent in developing diagnostic methods to measure the electric and magnetic fields in the gun. Detailed plots of B_θ and E_z were made from which the ion density and ion velocity were deduced under the assumptions that the electrons were the main current carriers and that there was no radial plasma motion. The conclusion drawn from these measurements was that an ionization wave was propagating in the accelerator, imparting some forward momentum to the ions but generally insufficient to cause significant mass accumulation in the current sheet. We now believe that the assumptions outlined above are not valid, that ion current may be important, and that the plasma is either brought to the velocity of the current sheet, or driven into the electrodes.

In order to obtain better matching between the plasma mass and the electrical parameters, the energy storage capacitance was increased to five μfarads. This change increased the energy transfer to the plasma significantly.

At the beginning of the second year an unknown change in the gas valve caused an instability to occur in the current sheet; in this instability the sheet, which is initially azimuthally symmetric, collapses into a single localized spoke. After several months of investigation it was concluded that the occurrence of this instability depended upon the neutral gas distribution and did not occur if the current sheet continually swept up gas.[2]

After the instability problem was resolved an energy inventory was taken which showed that 65% of the initial stored energy was being delivered to the accelerator. The work done on the current sheet could not be included in this inventory because the sheet was poorly defined until after the breech voltage reversed polarity. The broad current distribution was thought to indicate that the plasma was highly resistive and we postulated that there was a severe energy loss incurring during the first few tenths of a microsecond of the discharge period. This hypothesis seemed to be borne out by calorimetric measurements on the exhaust which gave a thermal efficiency of only 20%.

In recent measurements, with a pulse-line energy source, we have demonstrated unequivocally that ohmic losses are small and that most of the energy delivered to the accelerator does work on the current sheet. The low exhaust efficiency is thought to arise from radiation losses and direct loss of plasma to the electrodes.

At the beginning of the current contractual period, two guns with increased capacitance were made; the object was to increase the discharge period but because of the lower inductance it did not increase appreciably. At the end of the second year the overall electrical efficiency was 25% and a large test facility was built so that the behavior of the gun in repetitive operation could be studied if future development warranted it.

2.0 Description of the Equipment and Apparatus

The plasma accelerator, illustrated schematically in Fig. 1, is essentially the same as the one used in previous contracts. The propellant

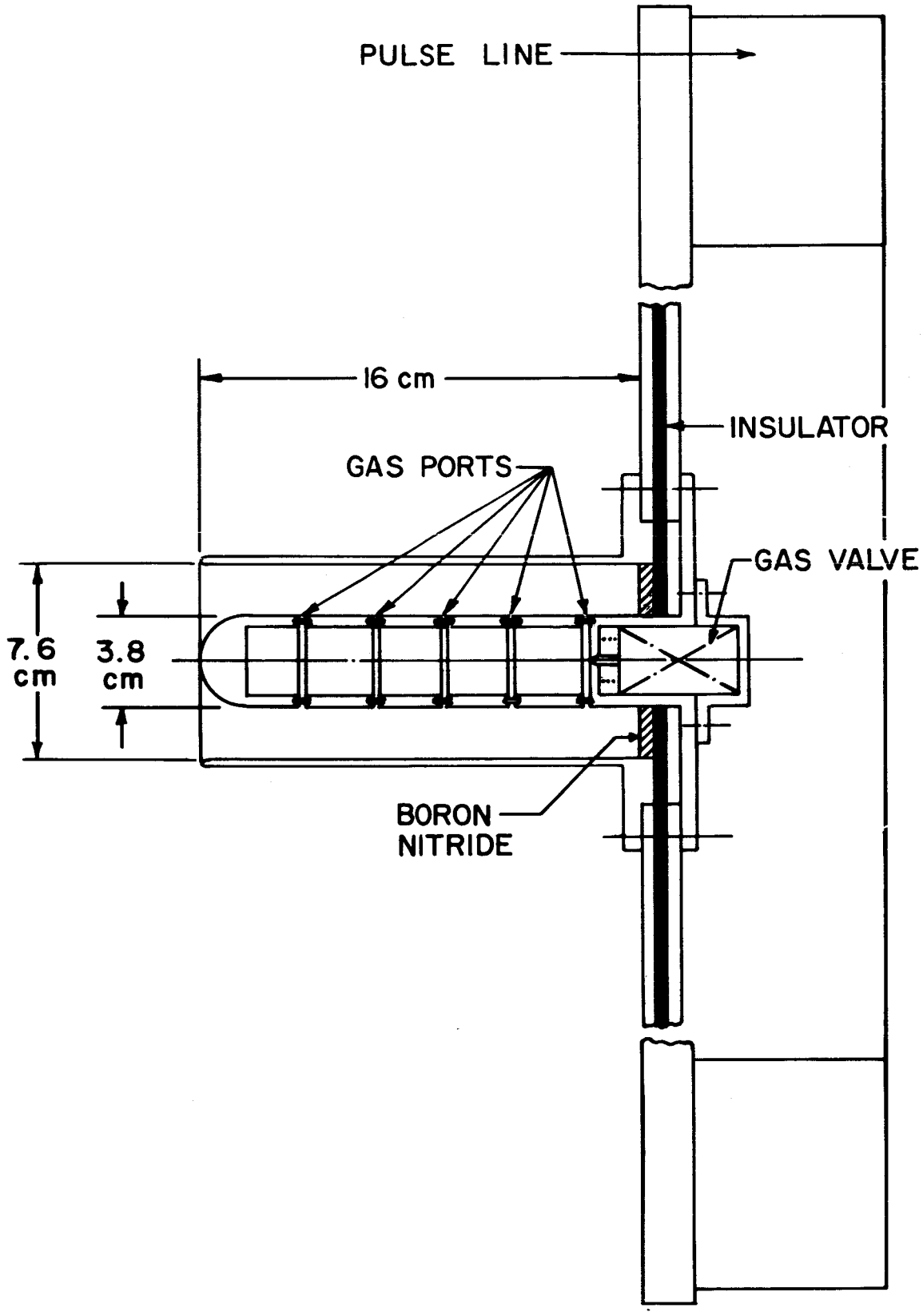

FIG. 1: SCHEMATIC DIAGRAM OF THE GUN

gas is fed through an electrically operated gas-valve mounted inside the inner electrode. We have made no attempt up to the present time to obtain good propellant utilization. The operating procedure is to charge the capacitor, and then pulse the gas valve so that breakdown occurs.

Three capacitor assemblies, designated Mark 7, 8, and 9, have been used during the year. The Mark 7, contains 15 capacitors each 0.8 μfarads; the total source inductance up to and including the insulator is 1.5 nanohenrys. The Mark 8 gun, shown in Fig. 2, was designed to accommodate 24 capacitors each 0.4 μfarad with 17 nanohenrys inductance, but has been operated with only 20 units because of capacitor failures. The source inductance including the insulator is also 1.5 nanohenrys.

The Mark 9 capacitor was designed and fabricated at GD/Astronautics because commercial capacitors were not designed for our application, and were unreliable, expensive, and difficult to obtain. The prototype unit, shown in Figs. 3 and 4, is a 22 μf, 4 nanohenry, 10 kv capacitor fabricated as a single torus 20" I.D., 22" O.D. and 11" long. It has more capacity yet is considerably smaller and lighter than the Mark 7 and 8 assemblies (~ 150 pounds weight compared with ~ 600 pounds). When the Mark 9 capacitor was discharged into the coaxial gun we discovered that it was behaving as a distributed parameter pulse-line rather than a single capacitor. Later, we realized that this behavior is common to most low inductance capacitors; however, it is not generally noticed because of the short pulse time and the relatively high load inductance.

The realization that a capacitor can behave as a transmission line is important to our program because an energy source can be made in

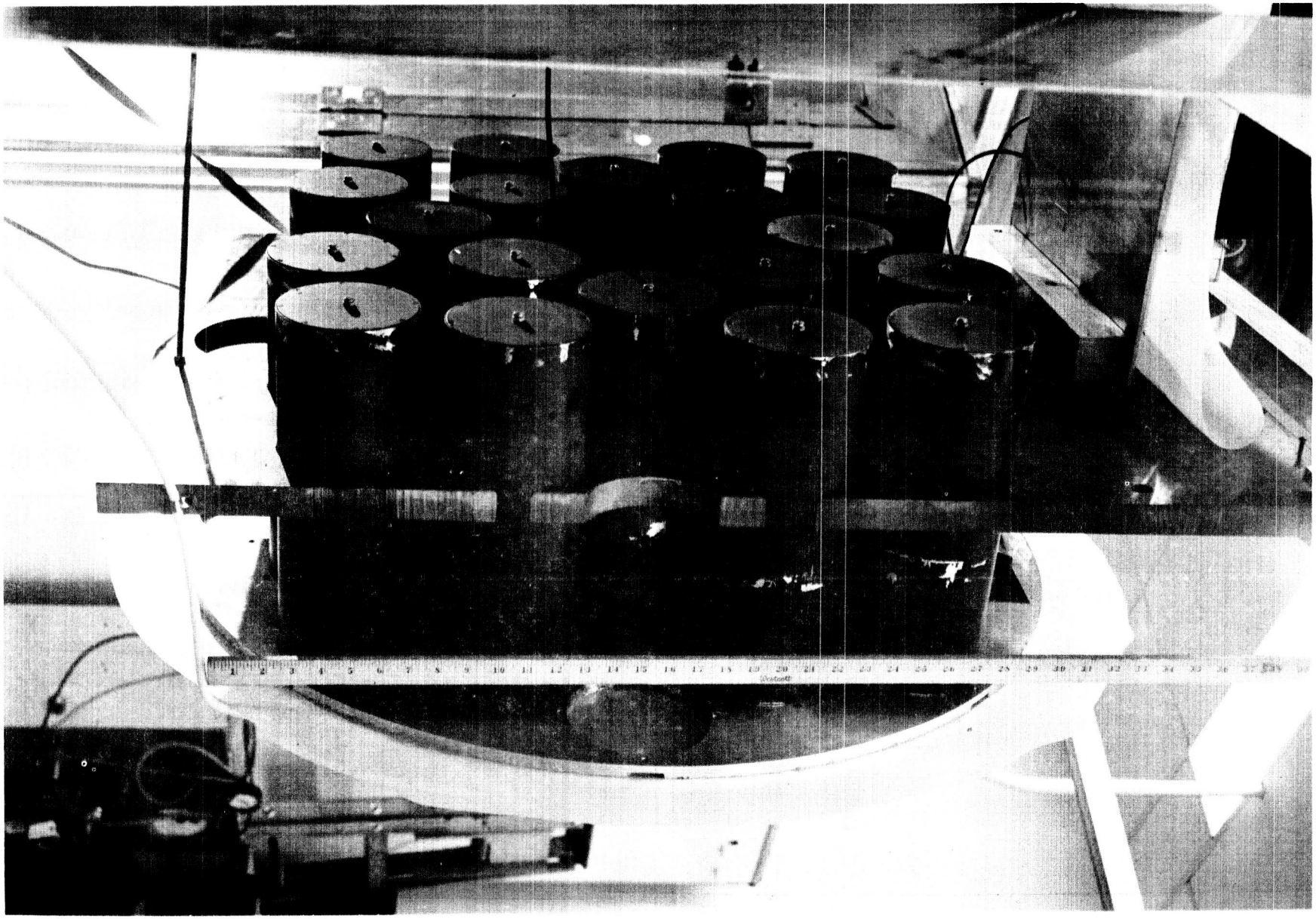

FIG. 2: MARK VIII CAPACITOR ASSEMBLY, C = 8.2 μF

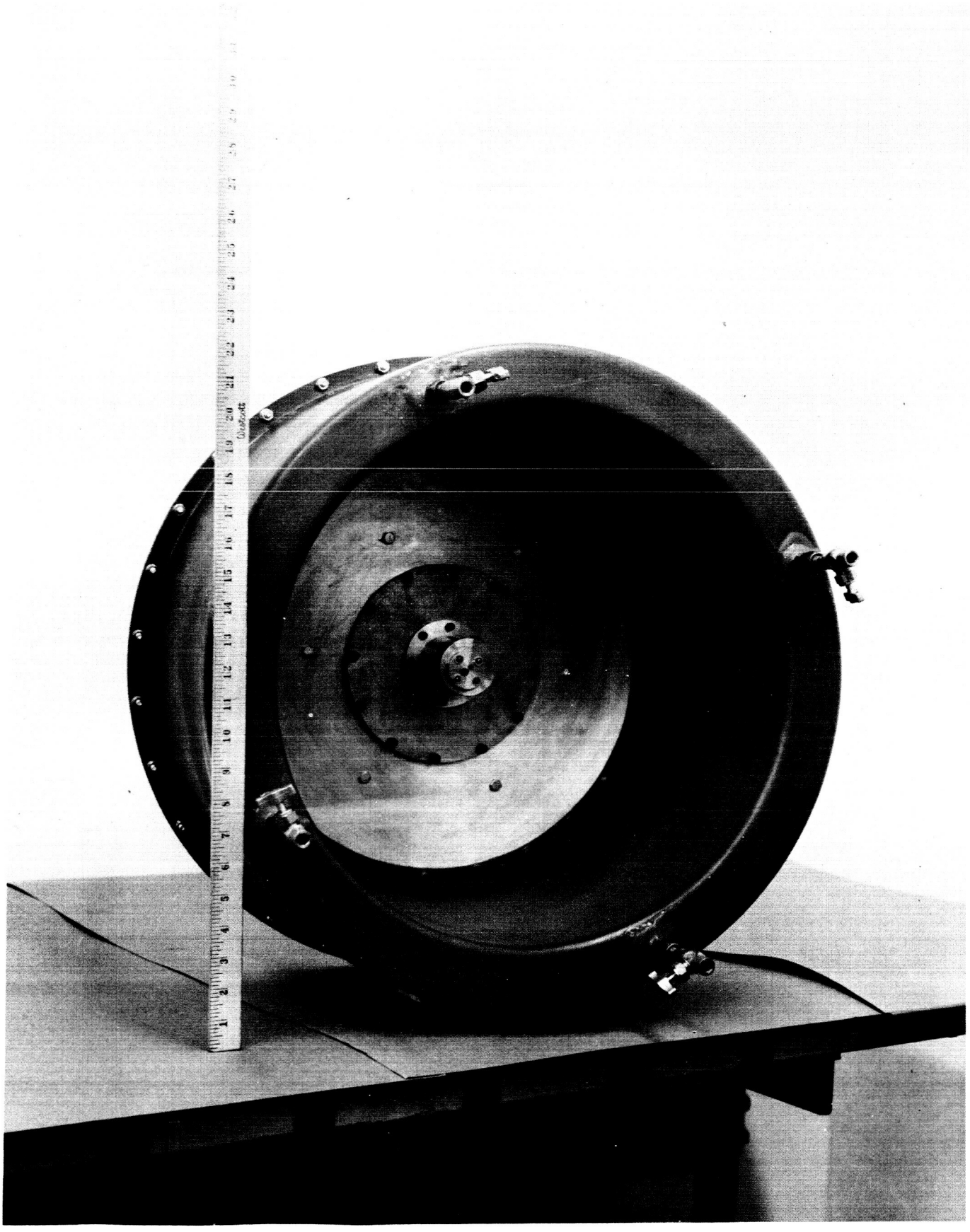

FIG.3: MARK IX PULSE LINE, REAR VIEW

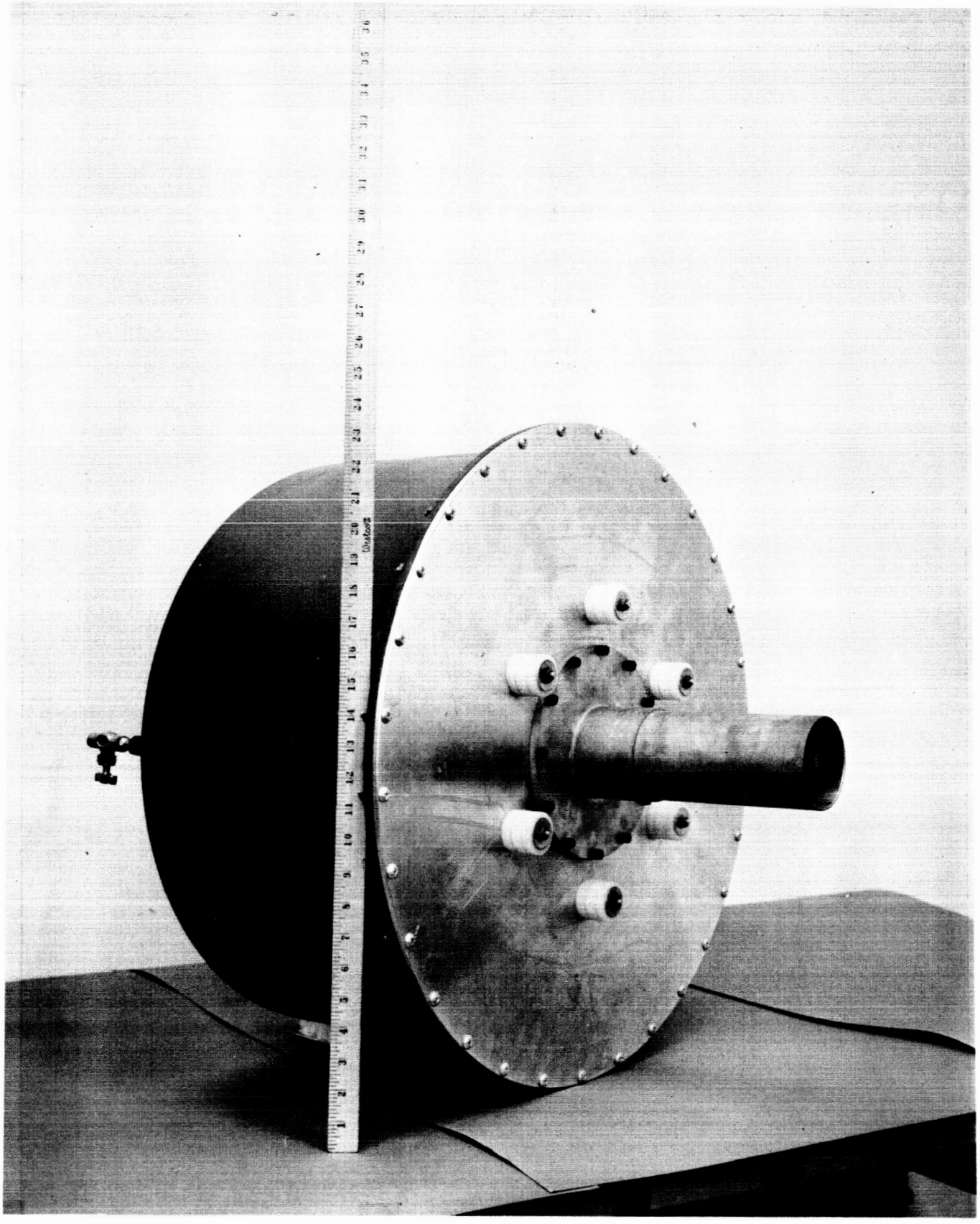

FIG. 4: MARK IX PULSE LINE, C = 22 μF

which the impedance is independent of the period chosen; this subject and the development program which has evolved is described in Appendix III.

Early this year GD/Astronautics completed the installation of a large test facility containing a stainless steel vacuum chamber - 6' in diameter by 14' long, with two 36" diffusion pumps backed by an ejector pump - a 150 kw high-voltage power supply and a large R.F. screened room. This facility is adequate for testing a propulsion unit at a power level of 100 kw while maintaining a base vacuum in the chamber of approximately 10^{-5} torr. All of the measurements described in this report were done at low power levels however (a few hundred watts maximum) to avoid engineering complications at this stage in the program.

3.0 Experimental Results

The experimental results are presented in two parts, one for the lumped capacitor guns and the other for the pulse-line type.

3.1 The Lumped Capacitor Guns

3.1.1 Electric and Magnetic Field Distribution

The distributions of B_θ and E_z in the Mark 7 and 8 guns were found to be essentially the same as those obtained previously in the lower capacity Mark 5 gun.[2] The current sheet forms on the insulator, then propagates at a velocity of 10 cm/μsec; the front of the current distribution is planar, in either polarity, and axial currents flow in the plasma behind the current sheet. A pulse of E_z accompanies the current front downstream; the time integral of E_z accounts for an ion velocity of a few cm/μsec, if the ions are assumed to be singly ionized.

A study of the radial electric field in the gun was made to determine the magnitude of the electrode sheath voltages. The experimental procedure was the same as for the E_z measurements, with the E probe tips spaced radially ($\Delta r = 0.55$ cm) rather than axially. The probe was moved radially across the interelectrode spacing at a fixed axial position, and also moved axially at a fixed radius.

Oscilloscope traces of E_r and B_θ are shown for an axial position $z = 10$ cm, at four radii, in Fig. 5. This data was taken with the 11.6 μf gun operated at 8.3 kV with the outer electrode positive and with nitrogen propellant. The rise in E_r is simultaneous with B_θ, within the limits of experimental error (the B_θ probe was located on the other side of the gun); behind the current sheet the magnitude of E_r is approximately equal to v x B where v = the current sheet speed. There is an E_r field ahead of the main current layer, however the total potential drop involved is less than a hundred volts. There is not a significant voltage sheath at the cathode.

It is illustrative to plot the axial distribution of E_r at a particular radial position, at a time when the current sheet has propagated some distance along the barrel. A typical case shown in Fig. 6 was obtained by making E_r measurements at mid-radius for various axial positions. The jump in E_r at the position of the current sheet is approximately equal to v x B; the field then decreases linearly crossing the axis at $z = 2.7$ cm. For axial positions of z less than 2.7 cm Poynting's Vector is toward the insulator at this time; the field energy between $z = 0$ and 2.7 cm is either being withdrawn and deposited in the capacitor, or is being absorbed in the 'resistance' of the second current sheet on the insulator.

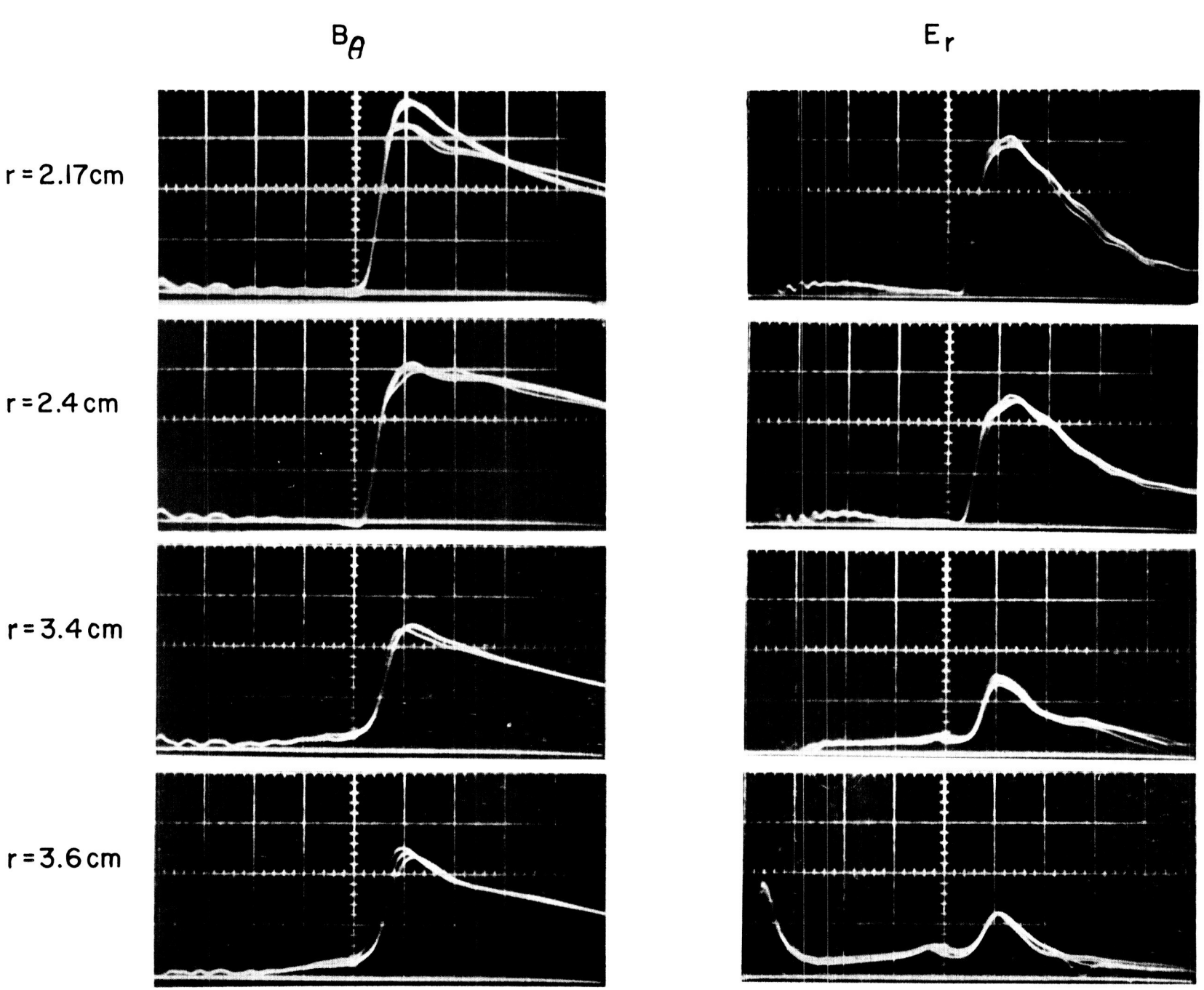

FIG.5 : OSCILLOGRAMS OF E_r and B_θ , B_θ = 2kG per cm,
E_r = 300 v/cm per cm , t = 0.2 μsec per cm

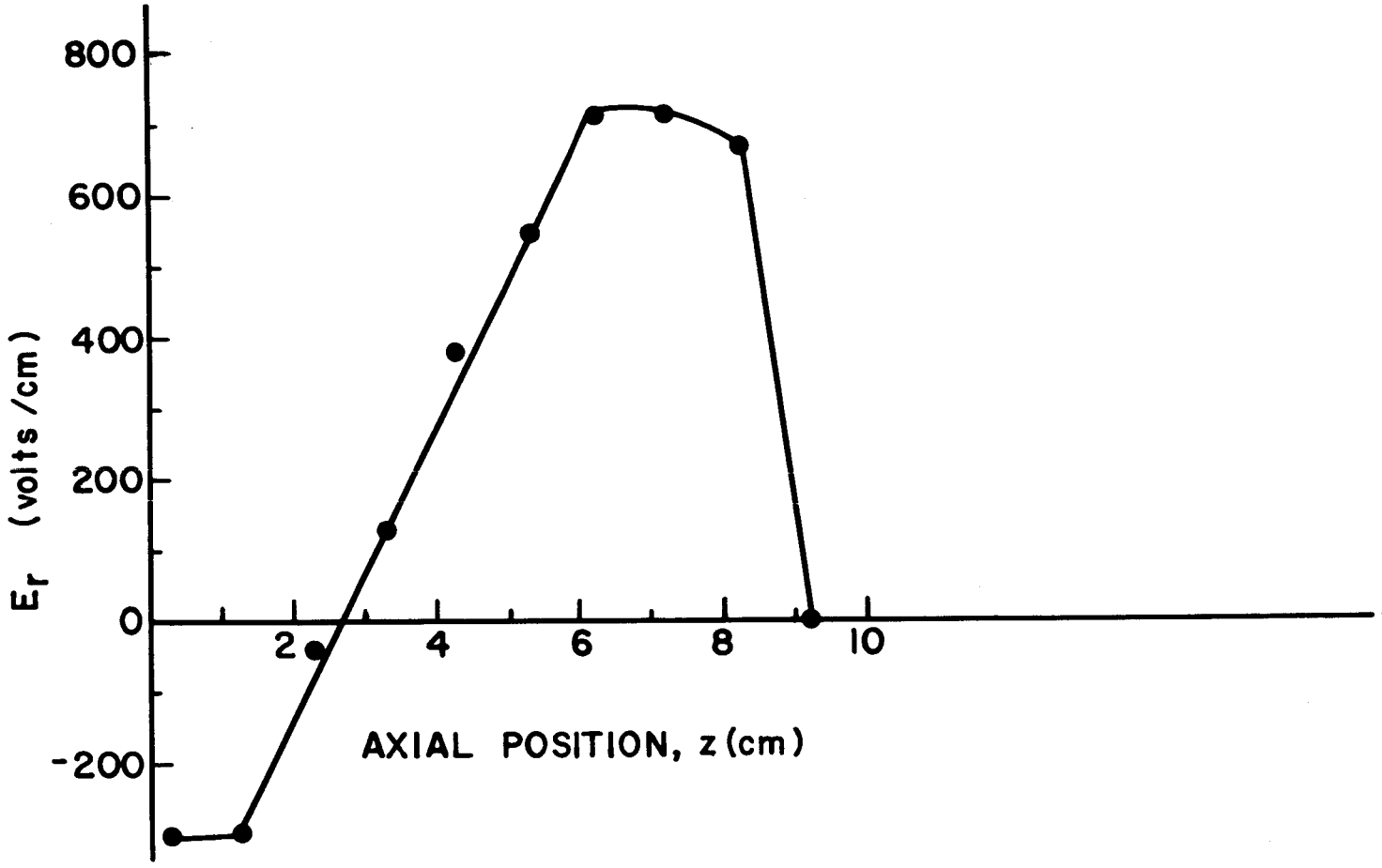

FIG.6. AXIAL DISTRIBUTION OF E_r AT $t=0.8\mu$sec
$r = 2.8$ cm

3.1.2 Energy Inventory and Efficiency Measurements

Breakdown in the gun can be made to occur at almost any position in the barrel by adjusting the pre-shot gas-density distribution. At low plenum pressures (approximately 100 torr) breakdown occurs on or near the insulator; at high plenum pressures (300 to 600 torr) it occurs about 6 cm out along the barrel. For the purpose of discussion, we will consider these conditions as two distinct operating modes; however, any intermediate situation could be attained by adjusting the gas port spacing.

The current and voltage waveforms (voltage measured at the capacitor terminals) for the two cases, shown in Fig. 7, are quite different because of the large difference in barrel inductance. At low pressures the waveform rises very fast and is asymmetric indicating that the inductance change during the first half cycle, caused by the motion of the plasma, is comparable to or greater than the source inductance. The waveform for the high plenum pressure rises more slowly, is also asymmetric and has a very sharp break at $t \sim 1.0$ μsec when the second discharge occurs back on the insulator.

We generally adjust the plenum pressure so that break-down will occur on the insulator, even though the overall efficiency is often higher when the initial break-down occurs downstream. There are two main objections to operating the gun in the latter mode; firstly, the tendency for spoke instability and, secondly, a subsequent breakdown must occur on the insulator at voltage reversal in order to trap field energy in the barrels.

An energy inventory, taken at the time the breech voltage crosses zero, is shown in the following table; this data, which is typical for both

CURRENT VOLTAGE

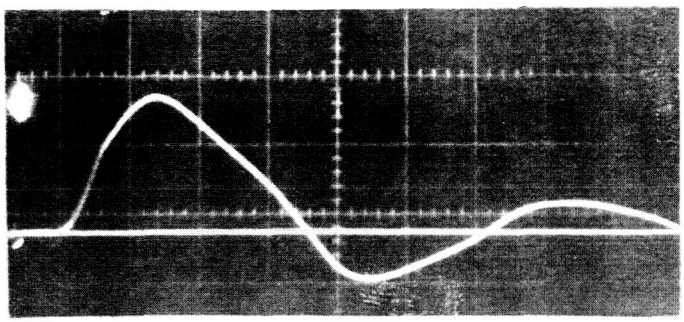

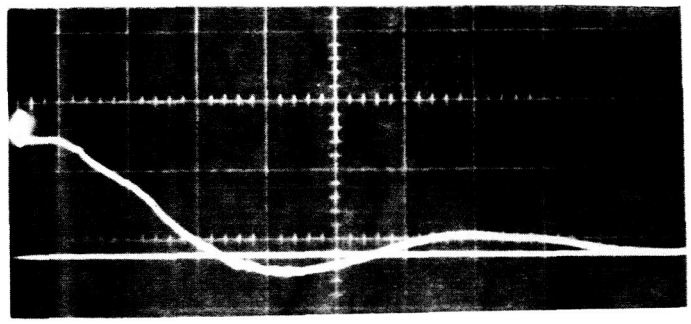

(1)

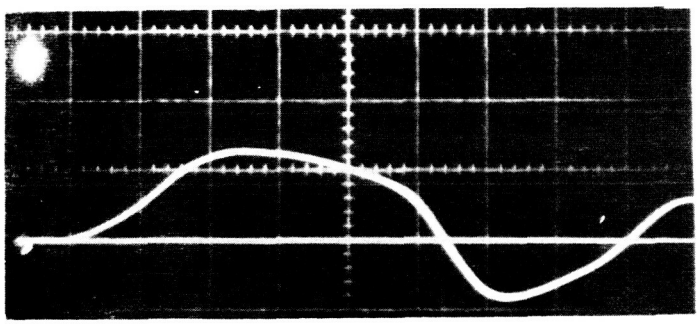

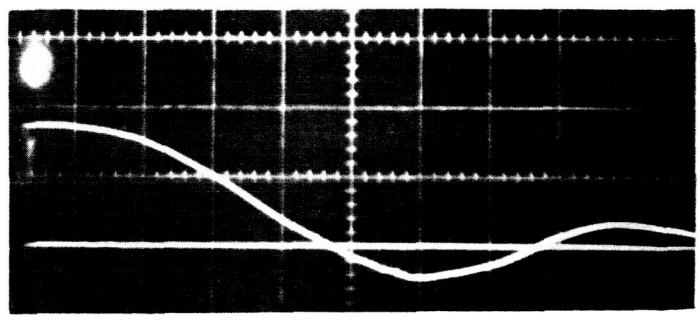

(2)

FIG.7: CURRENT AND VOLTAGE WAVEFORMS, LUMPED CAPACITOR GUN, I~160 kA per cm, V~5 kV per cm, t = 0.2 μsec per cm. (1) BREAKDOWN AT THE INSULATOR (2) BREAKDOWN IN THE BARRELS

the Mark 7 and 8 guns, was obtained with the Mark 7 gun using nitrogen with 7.8 kv on the capacitor. The breakdown occurred at the insulator.

Initial Stored Energy $\frac{1}{2} CV^2$ (11.6 μf at 7.8 kv)	= 354 joules
Electrostatic field energy remaining in capacitor at t = 0.45 μsecs	~ 1 joule
Magnetic field energy in capacitor	~ 36 joules
Energy input to gun $\int_0^{t = 0.45\ \mu sec} V \cdot I \cdot dt$	~ 307 joules
Magnetic field energy in barrels at t = 0.45 μsec	~ 97 joules

In the above case about 87% of the initial stored energy was deposited in the gun, of which only one third ever appeared as magnetic field. In the earlier Mark V gun, which has a lower capacity (5.5 μf) and higher inductance we found that for about the same stored energy 65% of the stored energy was deposited in the barrels and again only about one third ever appeared as magnetic field. The circuit equations and the partitioning of the input power between magnetic energy and work are discussed in Appendix I.

The calorimetric efficiency, which is defined as the ratio of the total energy collected in a calorimeter in the exhaust, to the initial stored energy, was measured at several voltages; the results are shown in Fig. 8.

3.2 Transmission Line Gun

3.2.1 Comments

The gun was built because we wanted to increase the energy-storage

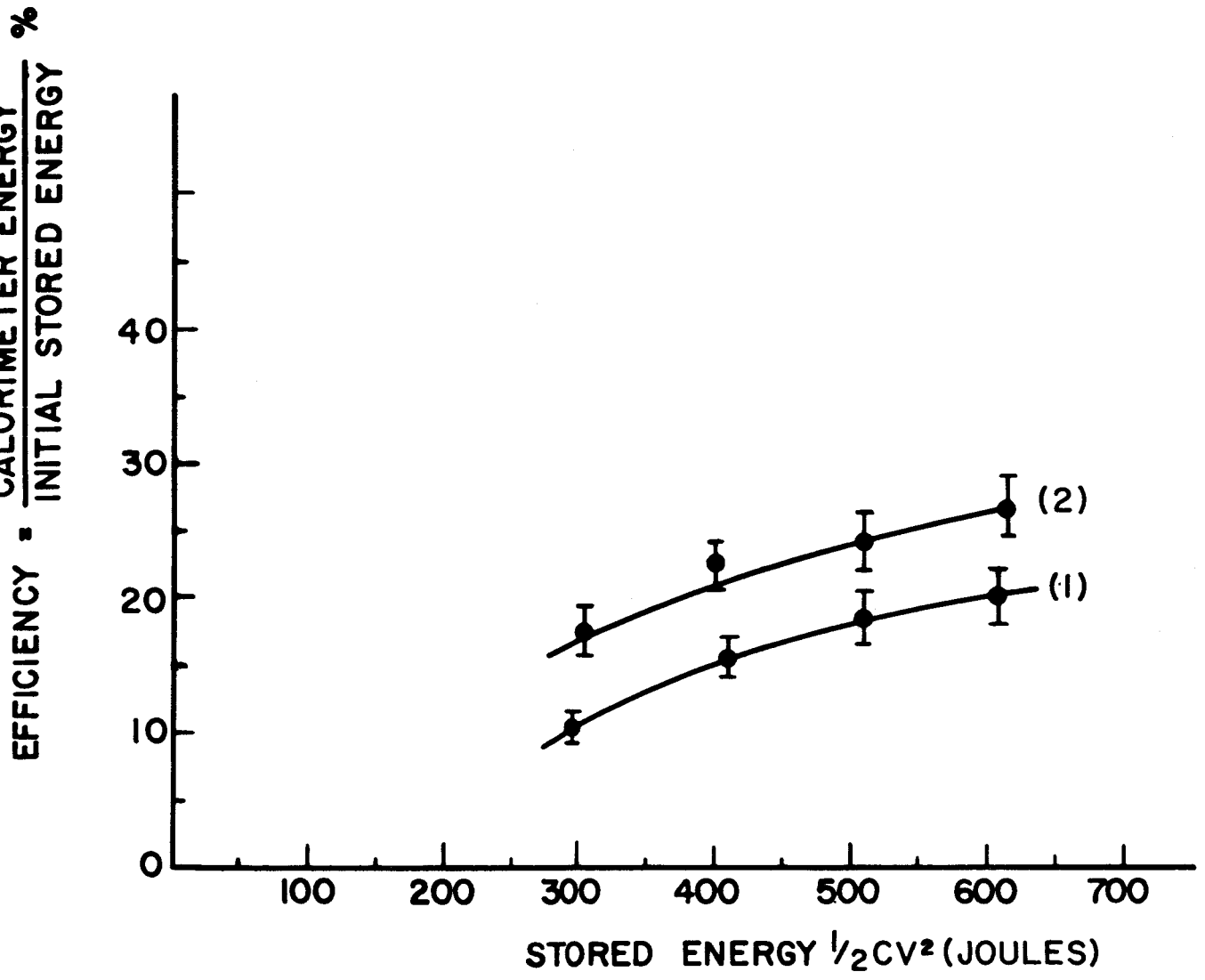

FIG. 8 : VARIATION OF EFFICIENCY WITH STORED ENERGY, LUMPED CAPACITOR GUN
(1) BREAKDOWN AT THE INSULATOR
(2) BREAKDOWN IN THE BARRELS

capacitance to lengthen the discharge period; the configuration shown in Figs. 3 and 4 was chosen because it was impractical to continue paralleling small capacitors. We did not realize that this method of construction would give a pulse-line behavior until the unit was discharged into the co-axial gun.

3.2.2 Energy Inventory

Oscillograms of the current to the gun, the voltage on the gun and the voltage at the open end of the pulse line are shown in Fig. 9. Nitrogen propellant was used and the gun was operated at 6.3 kv. The current rises to about 200 kA in 0.15 μsec and then remains essentially constant for 0.7 μsec; the voltage at the gun drops to slightly less than one half of the initial voltage and then swings negative at the time of arrival of the voltage wave reflected from the open end of the line; the voltage at the open end of the line is unchanged until the primary voltage wave arrives and reduces it to near zero. The waveforms demonstrate that after 0.15 μsec the impedance of the gun is very nearly constant at 14 mΩ.

The current sheet maintains azimuthal symmetry and the only significant component of magnetic field is B_θ; this was measured at three radii and at 1 cm intervals along the barrel. The B_θ oscillograms in Fig. 10 were taken at mid-radius; each photograph shows four successive traces overlaid. In Fig. 11 the axial distribution of B_θ at various times is plotted for the three radial positions. A clearly defined current sheet forms in a few tenths of a microsecond then travels along the barrels at a velocity of 10 cm per μsec.

From the data presented numerical values can be determined for lumped circuit parameters which describe the electrical behavior of the

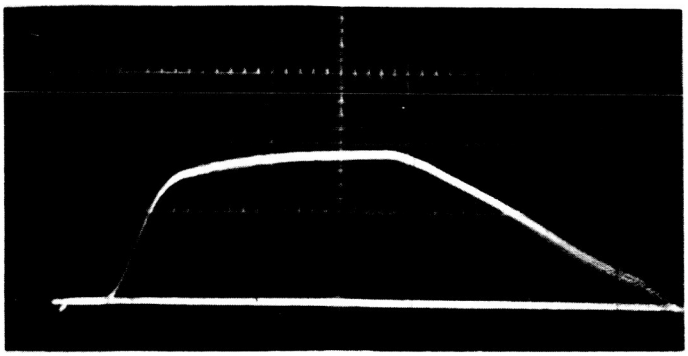

CURRENT

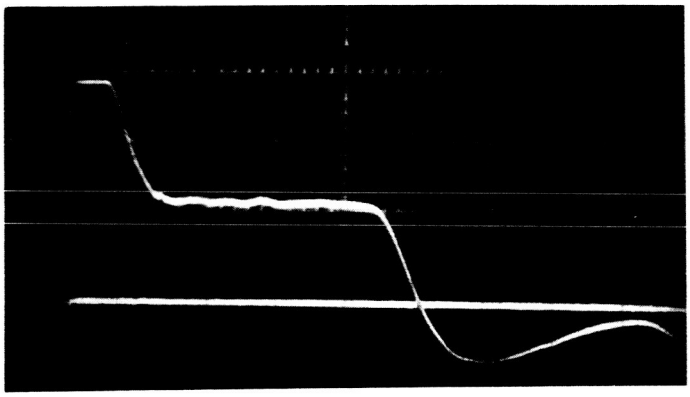

VOLTAGE ON
THE GUN

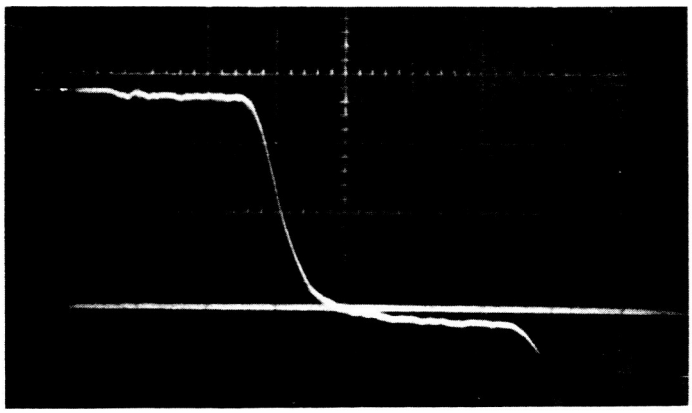

VOLTAGE AT THE
BACK OF THE
PULSE LINE

FIG. 9 : CURRENT AND VOLTAGE WAVEFORMS FOR PULSE LINE I $\sim 10^5$ AMP/cm, V $\sim$ 2 kV/cm t = 0.2 μsec/cm.

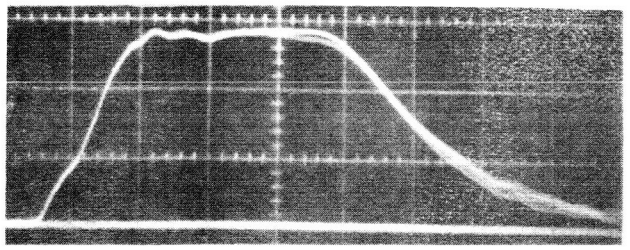

z = 0.5 cm

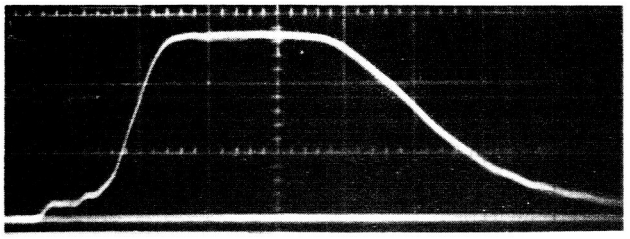

2.0 cm

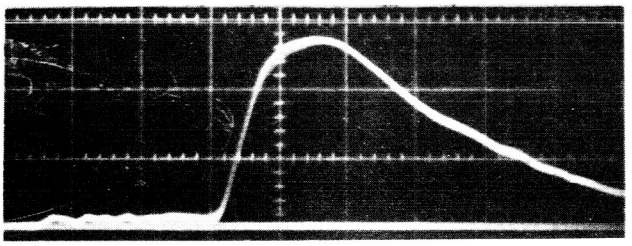

5.0 cm

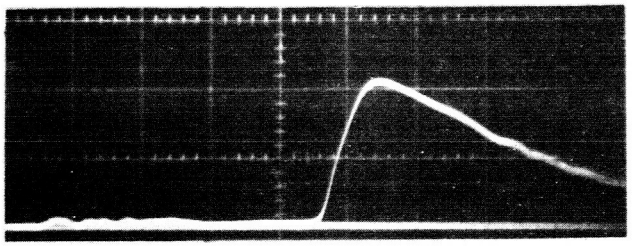

8.0 cm

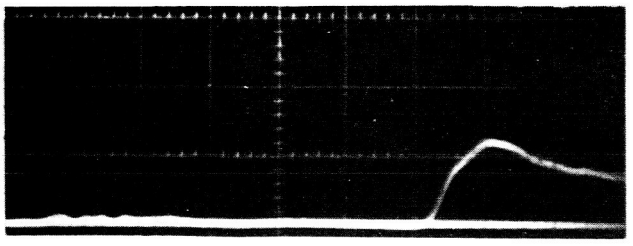

11.0 cm

FIG. 10: OSCILLOGRAMS OF B_θ, z = AXIAL POSITION
B_θ = 5.4 kG/cm , t = 0.2 μsec/cm .

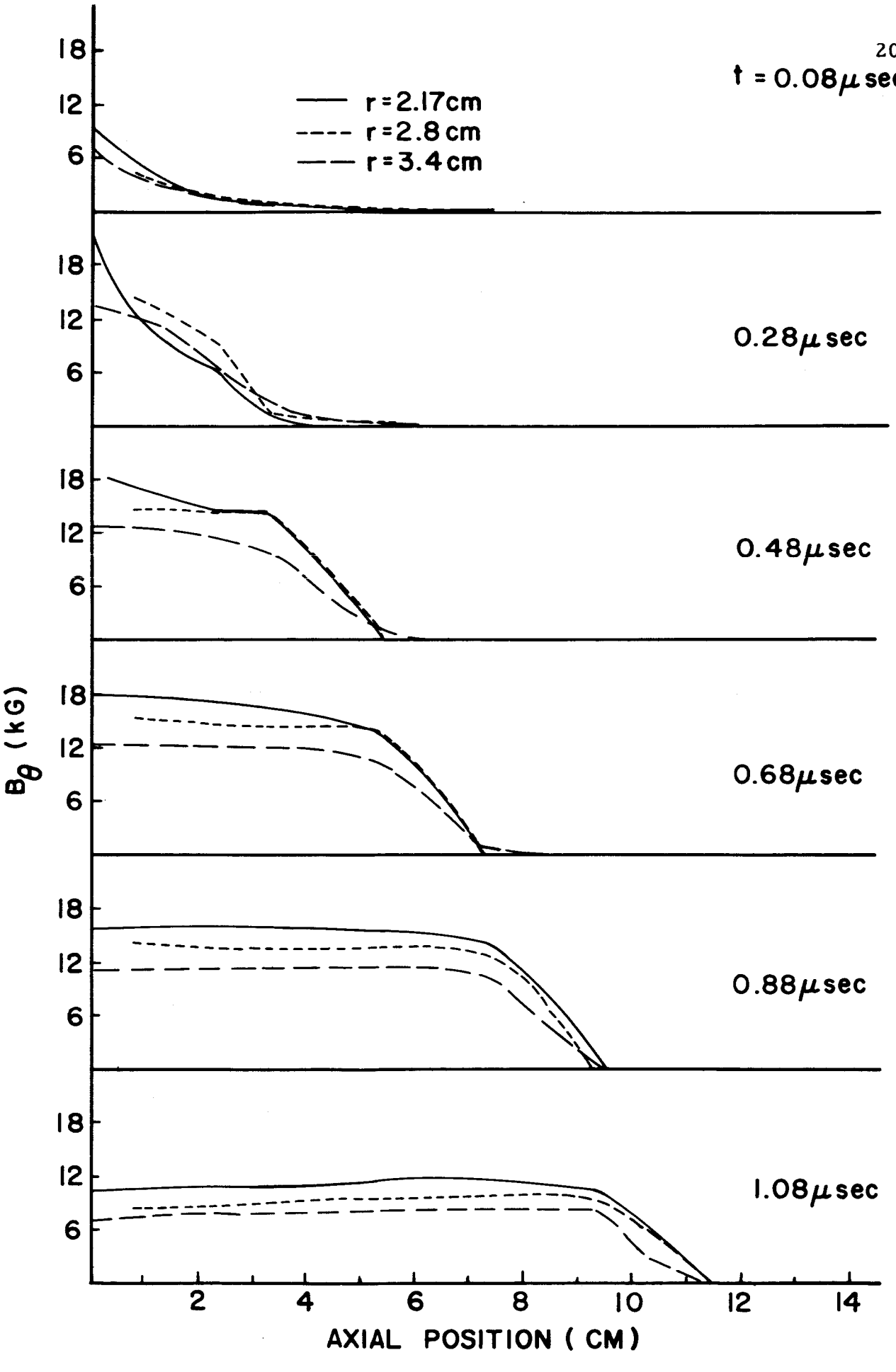

FIG.11 : AXIAL DISTRIBUTIONS OF B_θ, r = RADIUS

gun. The voltage at the terminals of the gun is given by the following equation:

$$V = \frac{d\phi}{dt} + IR = L\dot{I} + I(\dot{L} + R) \qquad (1)$$

It is permissible to talk of an inductance and its time derivative if the profile of the current sheet is steady and if the magnetic energy within the sheet is small compared with the total energy in the system. Figure 12 shows the sum $(\dot{L} + R)$ at different times; it was obtained by substituting in Equation (1) the measured values of I and $\dot{I}$, and a value for L calculated from the measured distribution of magnetic field. The inductance per unit length of the barrels is 1.4 nH/cm and, for a sheet speed of 10 cm/μsec, $\dot{L}$ is 14 mΩ; the data shows that the ohmic losses in the plasma are small.

By multiplying Eq. (1) by I we obtain an equation for the power input

$$P = VI = LI\dot{I} + I^2(\dot{L} + R)$$

$$= \frac{d}{dt}(1/2\, LI^2) + 1/2\, I^2\dot{L} + I^2R \qquad (2)$$

Integrating (2) gives the energy equation

$$\int_o^t P\, dt = 1/2\, LI^2 + 1/2 \int_o^t I^2\, \dot{L}\, dt + \int_o^t I^2R \qquad (3)$$

The first term on the right hand side is the magnetic energy inside the gun; this term finally must go to zero. The second term can be written as the time integral of the magnetic force acting on the current sheet

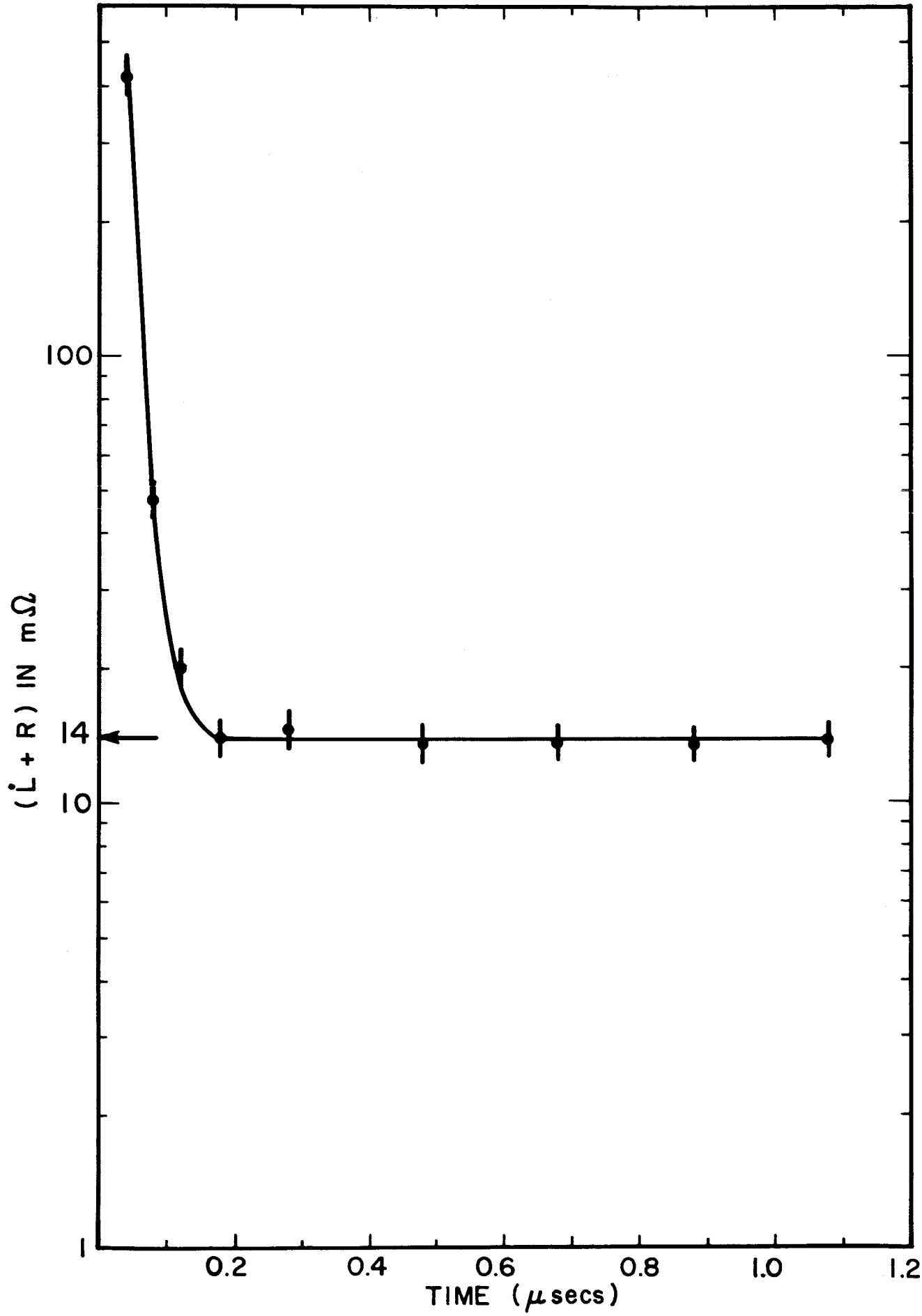

FIG. 12: TIME DEPENDANCE OF (L̇ + R)

multiplied by the sheet velocity; it equals the work done on the plasma and goes into kinetic energy, internal energy, and losses. The last term is the energy dissipated in ohmic losses and is much smaller than the other two terms. All the terms except the last can be calculated from the measurements described; Fig. 13 shows how they vary with time. 88% of the energy stored in the pulse line has been transferred to the gun at 0.8 μsec when voltage reversal occurs; up to this time the energy is shared approximately equally between the magnetic field and the work done on the current sheet. After voltage reversal some of the magnetic energy in the barrel is withdrawn and returns to the pulse line while the rest continues to do work on the current sheet. The total energy supplied to the gun is 69%, of which 58% can be identified as work done on the plasma. The difference is presumably due to resistive losses and experimental error.

3.2.3 Efficiency Measurements

The calorimetric efficiency was only 15%, but when the barrels were shortened from 16 cm to 9 cm it increased to 30%. The efficiency also increases with greater applied voltage and with larger outer barrel diameter. An efficiency of 45% has been achieved with an outer barrel diameter of 12.7 cm at an applied voltage of 7.8 kV using the Mark 9 pulse line with nitrogen propellant.

The variation of efficiency with voltage and barrel diameter is associated with the matching of the electrical period to the velocity of the current sheet and the barrel length. As the voltage is lowered the sheet speed is reduced, and it is found to be essential that the period

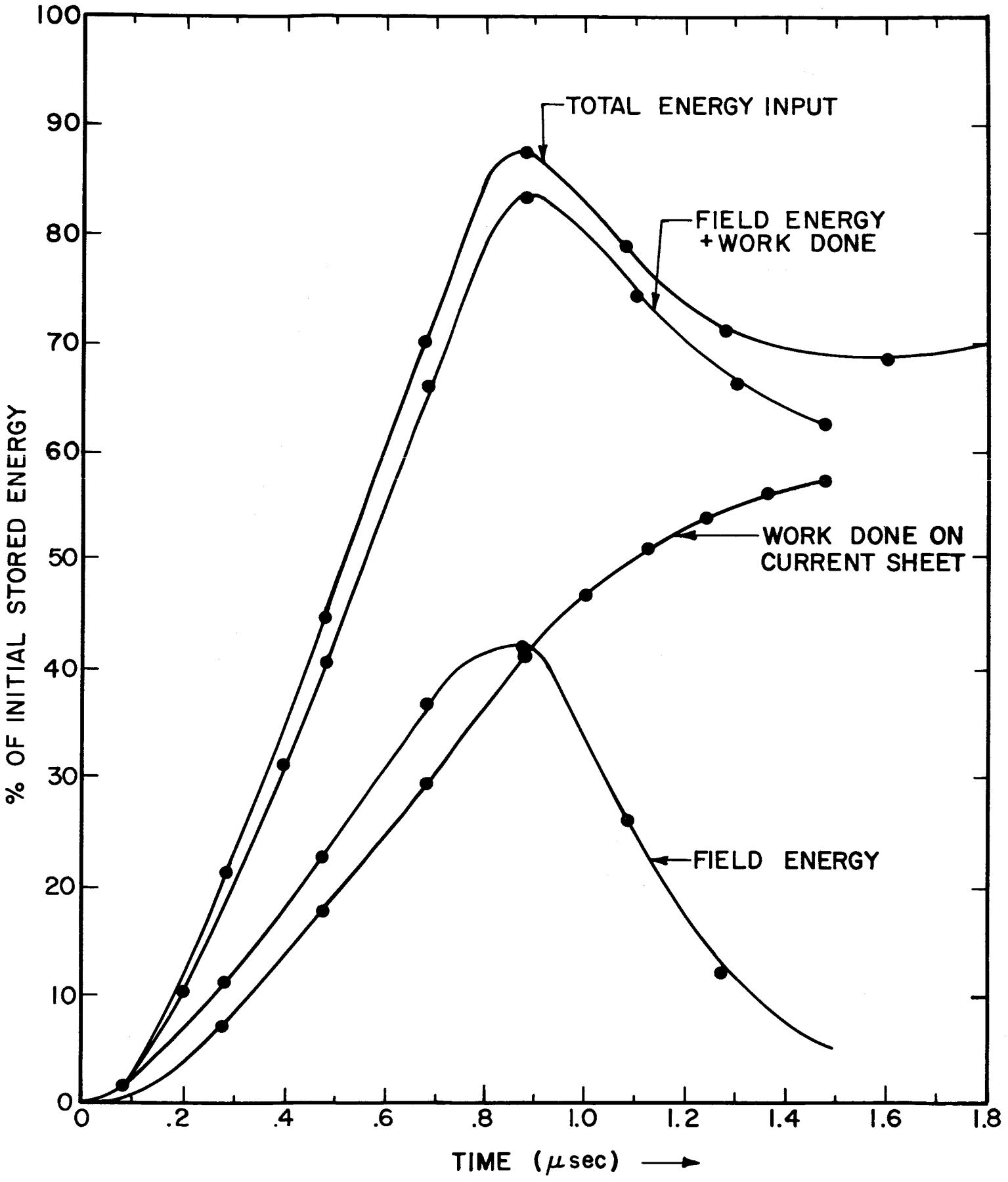

FIG. 13: ENERGY INVENTORY FOR THE PULSE LINE

be increased or the barrel length reduced in order to maintain high efficiency. In our previous measurements we have kept a fixed barrel length and electrical period and only approached optimum matching at the higher voltages. Measurements are now in progress to determine the scaling relationships between applied voltage, sheet speed and barrel length. The pulse-line energy source is invaluable in this work because impedance and pulse time can be varied independently.

4.0 Summary and Conclusions

The program during the past year has been, as in previous years, directed toward understanding the physical phenomena involved in the acceleration of plasma. We have deliberately avoided engineering problems associated with propellant utilization, operation at high power levels, and measurement of thrust, although we realize that these problems are very important from the standpoint of thrustor development. Considerable effort has gone into the development of diagnostic methods to examine the exhaust, and the improvement of the diagnostic techniques developed in earlier work.

We have tackled one of the outstanding engineering problems, the development of a low loss, light weight energy-storage capacitor. This program, which was started because commercial capacitors were hopelessly inadequate for our application, has worked out very well and has led to the development of a pulse-line energy source. This development is in itself a significant accomplishment and of major importance in pulsed plasma accelerator research.

Using a pulse-line energy source we made an accurate energy inventory for the accelerator which showed that a large fraction of the

initial stored energy was being converted into work on the first current sheet. We are now confident that the accelerator efficiency will not be limited by poor energy transfer from the energy source to the plasma. The inventory also demonstrated that the resistive losses that occur during the creation of the plasma are small and that the difficulties, which we encountered in balancing the energy inventory in an accelerator with a lumped capacitor energy source, arose because the current sheet was not well established before voltage reversal.

The thermal efficiency of the accelerator has been increased to 45% at an average exhaust velocity of about 7 cm per microsecond. We expect to maintain this efficiency at lower exhaust velocities by lengthening the acceleration period. However we do not expect to be able to increase the efficiency significantly with the present mode of operation.

Theoretical analysis shows that when a current sheet moves at constant velocity, into gas of uniform density, the energy supplied to the plasma partitions equally between the directed kinetic energy and the various forms of internal energy; the guns used presently operate in this mode. Furthermore, at the densities employed very little of the internal energy can be reclaimed by expansion because the electron temperature must be radiation-limited to 5-10 eV, and the electrons will then cool the ions in a time short compared with the acceleration period. (See Appendix I.)

It appears unlikely that efficiency in excess of 50% can be attained with the present distribution of neutral gas; however, higher efficiencies

are possible if the plasma is accelerated through vacuum rather than neutral gas. An alternative approach, which may also yield higher efficiencies, is to feed propellant into the breech of the gun at a sufficient rate so that the current sheet remains stationary while the plasma accelerates through it.

Appendix I Theoretical Discussion of Plasma Acceleration by Current Sheets

In this appendix some general features of plasma acceleration by current sheets are discussed. It is assumed that the magnetic field in the plasma is generated by unidirectional currents flowing in the plasma. The discussion applies to a one-dimensional system and is aimed primarily at pulsed coaxial accelerators.

I.1 Energy Partition in a Moving Current Sheet Accelerator

I.1.1 Magnetic Energy

When plasma is accelerated by a moving current sheet the energy supplied by the power source is partitioned between several different energy forms (i.e., magnetic, kinetic, internal and radiation). Initially the major division is between magnetic energy and the other energy sinks; this division can be analyzed as follows.

The voltage drop across the input terminals to the gun is given by

$$V = IR + \frac{d}{dt}(LI) \qquad (1)$$

where

L is the circuit inductance

I is the current flowing

R is circuit resistance

Strictly, Eq. (1) can only be used when the current is restricted to a thin sheet; in the case of a diffusing sheet integral field terms should be used in place of the circuit parameters I, L and R. However, the physical arguments are the same in both cases.

The power supplied to the gun is

$$P = VI = I^2R + \frac{d}{dt}(1/2\, LI^2) + 1/2\, I^2 \dot{L} \qquad (2)$$

Hence the energy which has been supplied at any time is

$$E = \int_o^t P\, dt = \int_o^t I^2 R\, dt + 1/2\, L(t)\, I^2(t) + 1/2 \int_o^t I^2 \dot{L}\, dt \qquad (3)$$

The first term represents the resistive losses in the accelerator and can usually be ignored. The second term is the magnetic energy within the accelerator at any time and finally equals zero. The third term gives the work done on the plasma; by the time the current ceases to flow this term has accounted for nearly all the energy retained by the gun.

Equation (2) may be written

$$P = I^2R + (LI\dot{I} + 1/2\, I^2 \dot{L}) + 1/2\, I^2 \dot{L} \qquad (4)$$

Equation (4) shows that initially, while the amplitude of the current is increasing, energy is given to the magnetic field at a faster rate than to the plasma; this follows because the magnetic energy term always exceeds the last term when $I\dot{I} > 0$. If a steady state is reached so that the current remains constant then energy is supplied to the magnetic field and the plasma at equal rates because $I\dot{I} = 0$. When the amplitude of the current begins to decrease more energy is given to the plasma than the magnetic field because $I\dot{I} < 0$. The total magnetic energy decreases when

$$-\dot{I} > I\dot{L}/2L \qquad (5)$$

and finally if

$$-\dot{I} > I\dot{L}/L \tag{6}$$

the voltage on the accelerator is reversed and magnetic energy is withdrawn. In practice this withdrawal of magnetic energy is usually stopped by breakdown across the surface of the insulator at the terminals of the accelerator which then become short-circuited. ("crowbar.") Energy is dissipated in this breakdown at the insulator which may erode as a result. A better way to get good utilization of the magnetic field energy is to keep

$$I\dot{L}/L > -\dot{I} > I\dot{L}/2L \tag{7}$$

for as long as possible after peak current; then the stored magnetic energy is used to drive the plasma and is not withdrawn. In principle this condition can be satisfied by the correct choice of the circuit elements which constitute the energy source.

I.1.2 Directed Kinetic Energy

Of the energy which goes into the plasma not all need appear as directed kinetic energy; the partition between kinetic energy and other energy forms is determined principally by the distribution of neutral gas ahead of the current sheet. The energy partition depends to a lesser extent upon the detailed behavior of the plasma; in particular if any portion of the plasma expands then its thermal energy may be converted into directed energy. Two extreme cases are usually considered:

1) The 'slug' model[3]

2) The 'shock' model[4,5]

In the 'slug' model it is assumed that the current sheet has some initial mass associated with it which remains constant during acceleration; in this case all the work done by the moving current sheet goes into directed kinetic energy as long as the density profile remains constant. In the 'shock' model the current sheet moves into neutral gas of uniform density and sweeps it up. The energy partition depends on the detailed behavior of the plasma and is complicated because expansion can cause thermal energy to be converted into directed energy. However the effect of a velocity difference between the plasma and the current sheet can easily be demonstrated.

For simplicity assume that the current sheet is moving at a constant velocity. Gas is swept up at the rate $\rho_o v_s$ per unit area, where ρ_o is the uniform density ahead of the sheet and v_s is the velocity of the front which separates the moving gas from the stationary gas. (In the case of the 'snow-plow' model v_s is equal to the current sheet velocity v_c). It follows that the rate at which the moving plasma gains momentum is $\rho_o v_s v_p$, where v_p is the directed velocity given to the plasma by the current sheet. The force per unit area on the sheet is equated to the rate of change of momentum

$$B^2/2\mu_o = \rho_o v_p v_s \tag{8}$$

Similarly the rate at which work is done on the plasma is

$$v_c B^2/2\mu_o = 1/2\, \rho_o v_s v_p^2 + P_I \tag{9}$$

(The first term is equivalent to $1/2\, I^2 \dot{L}$, the second term is the rate at which the sheet gains kinetic energy and P_I is the rate at which internal energy is given to the plasma.)

From equations (8) and (9)

$$P_I = \rho_o v_s v_p (v_c - v_p/2) \tag{10}$$

Equation (10) shows that

1) If $v_p = 2v_c$ then P_I is equal to zero.

2) If $v_p = v_c$ then P_I is equal to the rate at which energy is given to directed motion.

3) If $v_p < v_c$ then P_I exceeds the rate at which energy is given to directed motion.

If $v_p = 2v_c$ the current sheet elastically reflects the gas as it is swept up. The only current sheet accelerating mechanism which satisfies this condition is one suggested by Rosenbluth;[6] this model requires a collision-free current sheet with fully-ionized gas ahead of it and has never been demonstrated experimentally. It is probably of academic interest only. The case in which the plasma is accelerated to the sheet speed is of most practical interest. The third case describes the 'leaky piston' which always is inefficient.

I.1.3 Internal Energy

Equation (10) shows that if $v_p = v_c$ the total internal energy given to the plasma is

$$\int_o^t P_I \, dt = 1/2 \int_o^t \rho_o v_p^2 v_s \, dt \tag{11}$$

In the interests of clarity the discussion so far has been concerned with a uniform neutral density and a current sheet moving with a constant

velocity. Insight into the more realistic case of an accelerating current sheet which moves like a snow-plow into a non-uniform gas density can be gained by the following physical argument. To an observer moving with the current sheet the neutral gas streaming into the current sheet has a kinetic energy per unit cross-section of $1/2\ \rho_o\ v_p^2$; all of this kinetic energy is dissipated in internal energy as the plasma is brought to rest. The internal energy is an invariant to a velocity transformation and consequently is the same for an observer in the laboratory frame. The rate at which the internal energy is supplied to the plasma at any moment depends on v_s and is simply $1/2\ \rho_o\ v_p^2\ v_s$ if we assume that none of the internal energy is subsequently transformed; then Eq. (11) follows by integration. In brief internal energy is generated if the current sheet sweeps up stationary gas; more precisely it is produced whenever the particle density is increased.

Initially the internal energy is in thermal motion but later it may be transformed as a result of collisions. In principle the energy in thermal motion can be converted into directed motion given the correct expansion cycle. However there are two attendant difficulties: firstly, for high conversion efficiency a nozzle is required which will reflect the expanding plasma and, secondly, the expansion process must take place before a major part of the thermal energy is transformed by inelastic collisions. In the plasmas commonly encountered in propulsion, the internal energy will be lost to excitation or radiation in less than one microsecond. The following example illustrates the latter point.

Consider a nitrogen plasma of electron density $10^{16}\ cm^{-3}$, containing 10^{18} ions, into which power is fed at a rate of 10^8 watts. (These

figures roughly apply to the coaxial accelerator described in this report.) Although the transient atomic processes within energetic hydrogen plasmas containing traces of heavier elements have been considered in connection with controlled fusion[7, 8] plasmas composed entirely of heavier elements have not received the same attention. However general conclusions can be drawn by considering the rates of the major processes. The excitation energies of the strongest transitions in nitrogen ions up to N^{VI} are all about 10 eV; the excitation coefficient corresponding to this energy can be calculated from the approximate relation.[8]

$$S = \frac{1.6 \times 10^{-6}}{\chi T_e^{1/2}} \exp\left(-\frac{\chi}{T_e}\right) \text{cm}^3 \text{ sec}^{-1} \qquad (12)$$

S is the excitation rate

χ is the excitation energy in eV

T_e is the electron temperature in eV

If T_e is taken to be 5 eV then the excitation coefficient is 10^{-8} cm^3 sec^{-1}. By definition

$$\dot{n}_{j+1} = n_e n_j S \qquad (13)$$

where n_e is the electron density and n_j is the density of ion in the jth excited state. Hence the power going into excitation per unit volume is

$$\dot{n}_j \chi = n_e n_j \chi S \qquad (14)$$

and the total power absorbed in excitation is 1.6×10^8 watts which is approximately equal to the input power; if a temperature of 10 eV is assumed the excitation rate doubles and the power required exceeds that available. In short excitation processes proceed at a rate, determined by the power available, and limit the electron temperature to the range 5-10 eV. The preceding argument has ignored the fate of the energy taken by excitation; if the plasma is transparent to the radiation this energy will be radiated, if however the radiation is trapped by resonance absorbtion the excitation energy is merely the first step in the cascade process which leads to the ionization of that particular species of ion or to radiation from a higher excited level. In either event the energy cannot be reclaimed and the electron temperature is limited to 5-10 eV unless subsequent excitation levels are considerably higher than 10 eV.

Whether the internal energy of the plasma is created initially in electron motion or in ion motion depends on the physical mechanisms in the shock and current sheet; however, we have seen that if the energy goes into electron temperature it is rapidly lost as a result of inelastic collisions. It will now be shown that if the internal energy is originally in ion motion it will rapidly be transferred to the electrons and consequently will also be dissipated by inelastic collisions.

In a plasma energetic ions will lose energy exponentially to cold electrons as a result of coulomb collisions. If the ion energy is much greater than the electron energy then:[9]

$$W = W_o \exp(-t/\tau) \tag{15}$$

where τ is given by

$$\tau = \frac{3\, m_e^{1/2}\, (k T_e)^{3/2}}{8\, (2\pi)^{1/2}\, n_e\, e^4\, Z^2} \cdot \frac{m_i}{m_e} \cdot \frac{1}{\ln \Lambda} \tag{16}$$

$$= 1.7 \times 10^7 \frac{T_e^{3/2}\, A}{n_e\, Z^2} \text{ sec}$$

T_e is the electron temperature in eV, n_e is the electron density in cm^{-3}, and A is the atomic weight of the ions and Ze is the ionic charge.

For a nitrogen plasma of density 10^{16} cm^{-3} and electron temperature 5 eV the relaxation time τ is 0.27 μsec. In one microsecond ions with an energy of 500 eV will be cooled to 12 eV by coulomb collisions with the electrons; the energy transferred to the electrons in this process will be subsequently lost in radiation and excitation as a result of inelastic collisions with the ions.

I.2 Plasma Acceleration by a Stationary Current Sheet

So far plasma acceleration by a moving current sheet has been discussed with particular reference to the partition of energy. Now we will consider briefly the main features of plasma acceleration by a stationary current sheet; this effect is considered for the sake of completeness and because it offers advantages over its moving current sheet counterpart.

An essential feature of the moving current sheet mechanism discussed in the previous section is that the mass accelerated is initially ahead of the current carrying region and subsequently is swept up as this region advances. In steady-state accelerators the current carrying

region remains stationary and neutral gas flowing into this region is accelerated by the magnetic body forces. Perhaps the best known accelerator of this type is the j x B accelerator which uses an externally applied magnetic field perpendicular to both the direction of the current flow and the direction of mass flow. An externally applied magnetic field is not an essential part of the stationary current sheet accelerator; this fact is demonstrated by the 'high performance' arc-jets in which the propulsive force is magnetic pressure and not particle pressure as in conventional arc-jets.

An interesting and illustrative physical picture of a stationary current sheet accelerator can be couched in terms of the moving-current sheet accelerator. Consider a coaxial gun supplied with a constant voltage; if a small 'slug' of gas is introduced at the breech then breakdown occurs and a discrete plasma is accelerated along the barrel. Suppose a fresh 'slug' is introduced after the first has moved a small distance along the barrel and this slug is followed shortly by another and so on. The barrel is quickly filled with a series of discrete plasmas each carrying current. If the interval between each plasma bunch is reduced towards zero then in the limit we have a stationary current distribution which is accelerating plasma. The only condition which must be satisfied is that mass is fed into the breech of the gun at an adequate rate.

The stationary current sheet accelerator has three main advantages over the moving current sheet accelerator.

1. Once the magnetic energy associated with the current sheet has been supplied, all the remaining energy can go to the plasma

unlike the case with the moving current sheet which, as a result of its movement, attempts to store an ever increasing amount of magnetic energy.

2. The particle density in any element of plasma decreases from the moment it enters the current sheet; because there is no compression there also is no need in principle to supply internal energy above that necessary for ionization.

3. In a moving current sheet accelerator plasma is ejected for a time t given by

$$t \sim \frac{\ell}{v_p} \tag{17}$$

where ℓ is the length of the barrels. The stationary current sheet accelerator has no corresponding limit to the time duration of the plasma pulse.

I.3 Accelerator Impedance

The electrical impedance of a current sheet accelerator is proportional to the sheet velocity if the magnetic field is produced solely by currents flowing in the plasma (i.e., for the case of no bias field). The impedance at constant current for the main types of current sheet accelerators are derived; this impedance is important as it determines the peak power level below which the accelerator will not function efficiently.

I.3.1 The Shock Model

In the 'shock' model of the moving current sheet accelerator the momentum equation is

$$B^2/2\mu_o = \rho_o v_p v_s$$

The power input to the accelerator at constant current is equal to twice the rate at which magnetic energy is generated and four times the rate at which the plasma is given kinetic energy; hence from Eq. (9) and Poynting's Vector

$$1/4\, EH = 1/2\, \rho_o v_s v_p^2 \tag{18}$$

From (8) and (18)

$$E/H = \mu_o v_p \text{ ohms} \tag{19}$$

E/H defines an impedance and can be related to the voltage and current required to accelerate plasma to a velocity v_p if the geometry of the accelerator is given.

I.3.2 The Slug Model

In the slug model of the moving current sheet accelerator the input energy is shared equally between magnetic and kinetic energy. Hence

$$1/2\, EH = \frac{\partial}{\partial t}(1/2\, M v_p^2) \tag{20}$$

and

$$B^2/2\mu_o = \frac{\partial}{\partial t}(M v_p) \tag{21}$$

because M, the total mass per unit area of the plasma slug, is constant

$$E/H = \mu_o v_p \text{ ohms} \tag{22}$$

I.3.3 The Stationary Current Sheet Accelerator

On the assumption that the input energy goes solely into directed

energy we have for the stationary current sheet accelerator

$$B^2/2\mu_o = \dot{M} v_p \tag{23}$$

and

$$EH = 1/2 \dot{M} v_p^2 \tag{24}$$

where $\dot{M}$ = the rate at which mass is supplied. Hence

$$E/H = 1/4 \mu_o v_p \text{ ohms} \tag{25}$$

Equations (19), (22) and (25) show that the electrical impedance of the principal current sheet accelerators differ by a factor four. For an exhaust velocity of 5×10^6 cm/sec a typical value of impedance is 5-10 milliohms. Because the applied voltage must exceed the electrode drop for efficient operation a minimum peak power is defined. Assuming that the source voltage is only 100 volts the peak power for an exhaust velocity of 5×10^6 cm/sec typically exceeds 1 MW, unless the magnetic field is produced externally.

Appendix II Diagnostics

II. 1 Ion Current Measurements Using Faraday Cups

Negatively biased Faraday Cups enclosed in grounded conducting shields have been used by several experimenters to determine ion density in streaming hydrogen plasmas;[10, 11] we have used this device for exhaust measurements on the co-axial gun with considerable success. Figure 14 shows a schematic diagram of a probe, the circuit used to bias the cup and a typical oscilloscope signal. The cup is biased sufficiently negative so that all the electrons in the plasma which enter the probe are repelled from the cup while the ions are collected. Under these conditions the ion current to the cup at any moment is

$$I = n e v A Z \tag{26}$$

where

n = the number density of the ions

e = the electronic charge

v = the component of ion velocity perpendicular to the face of the probe

A = the area of the hole in the ion probe

Z = the number of electronic charges per ion

The necessary bias voltage was determined experimentally by increasing it until all the electrons were repelled and the current collected ceased to increase; this occurred at approximately 20 volts and so the cups were normally biased to 45 volts. The bias required to repel the electrons depends not so much on the electron temperature

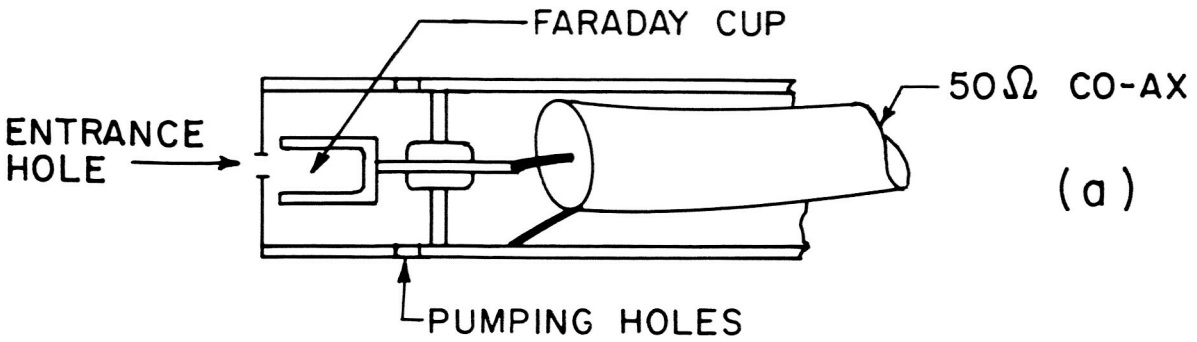

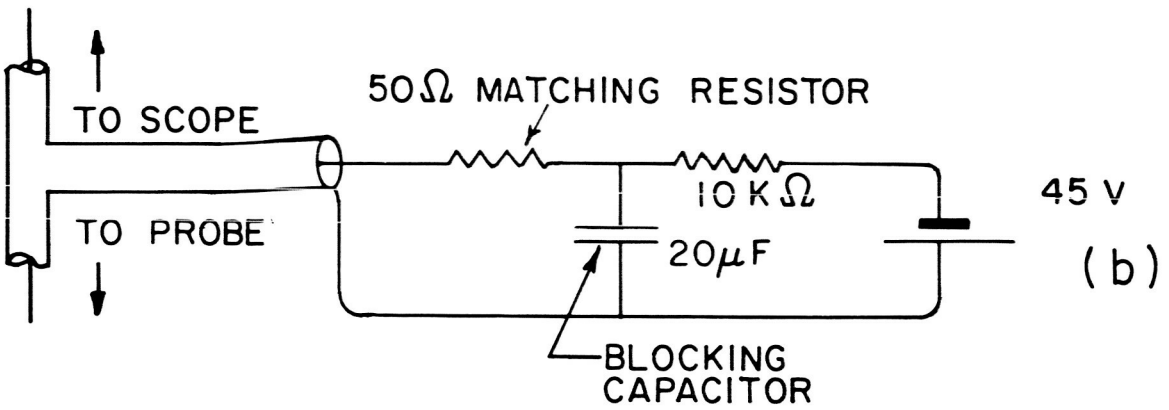

TYPICAL SIGNAL

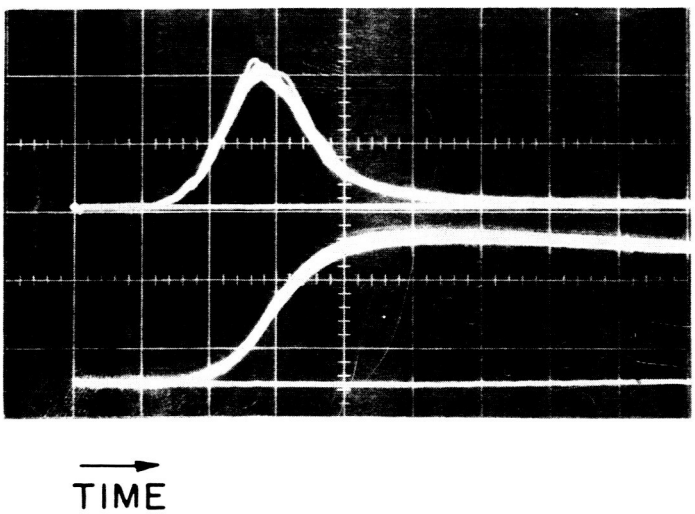

FIG. 14 : (a) ION PROBE (b) BIASING CIRCUIT
(c) TYPICAL SIGNAL 5 TRACE OVERLAY,
t = 10μ SEC PER CM., FLIGHT DISTANCE = 115 CM.
UPPER – UNINTEGRATED , LOWER – INTEGRATED

as the energy the electrons gain from stray electric fields near the accelerator. The hole diameter was varied from 0.05 mm to 1 mm to check the dependence of signal on hole size. Only the amplitude of the signal changed and Fig. 15 shows that this varied linearly with hole area as predicted by Eq. (26). The slight discrepancy shown by the smallest hole is within the experimental error involved in measuring the diameter of such a small hole. In both of the above experiments two adjacent ion probes were used simultaneously, the one acting as a monitor while the other had its bias voltage or hole size varied.

The dependence of ion current on the distance of the probe from the gun was also checked. Figure 16 shows how both the peak signal and the integrated signal depend on distance; as expected, the former decays inversely as the cube of distance while the latter decays inversely as the square. Distance was measured from the insulator at the breech of the gun. A 0.5 mm hole was used.

The ion density and velocity can be determined from the ion current; referring to Eq. (26) if Z is taken as unity then the only unknowns are n and v. Figure 16 shows that the gun behaves as a point source and as the plasma leaves the back insulator within 0.2 μsec, the directed velocity v can be measured by time-of-flight; with v known n can be determined by the magnitude of the ion current.

In the experiments described the ion density ranged from 3×10^{13} to less than 10^{11} cm^{-3} with ion velocities between 10^{6} and 10^{7} cm sec^{-1}. The main error is likely to be caused by secondary electron emission from the cup and by the presence of doubly ionized ions. At the moment

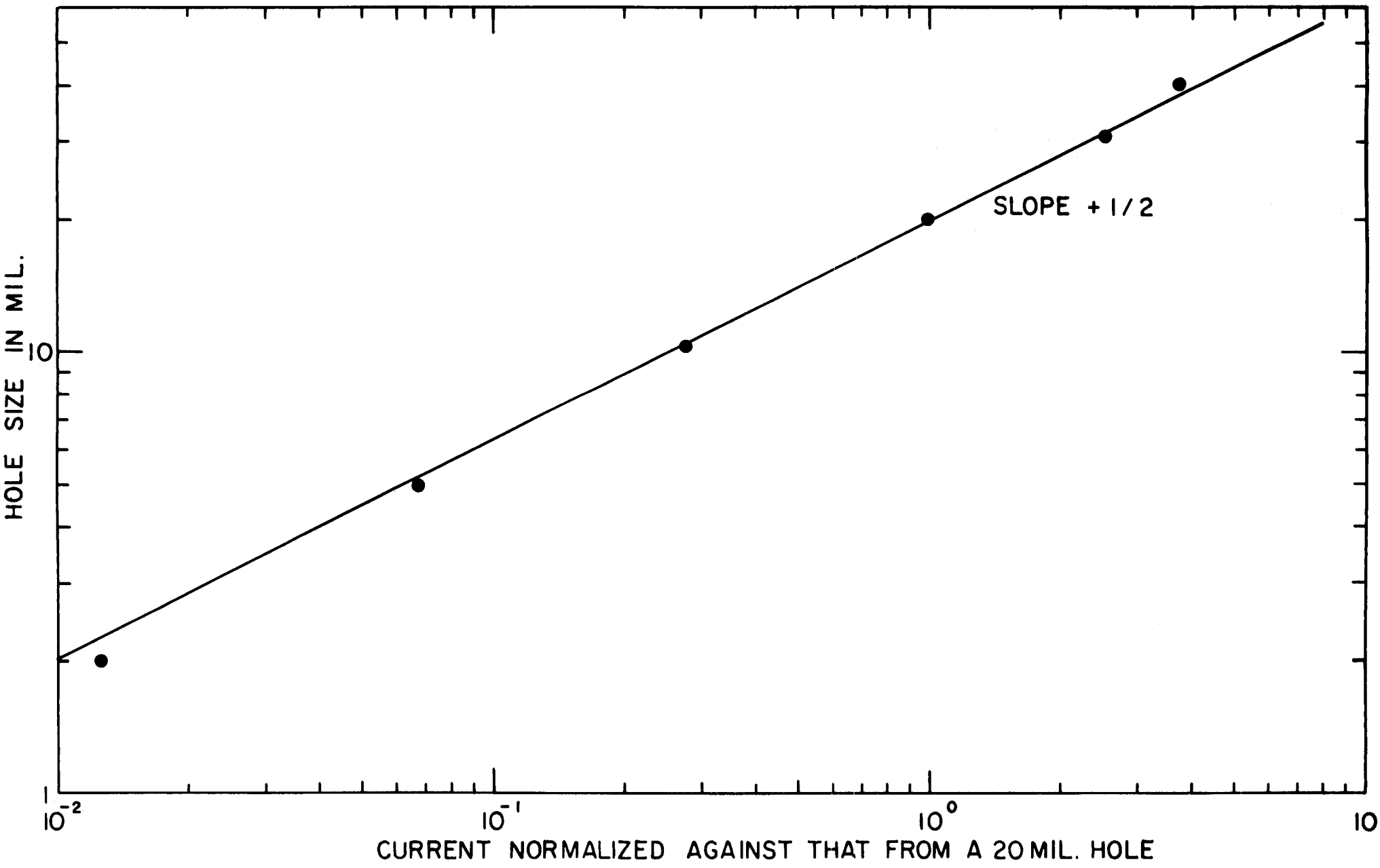

FIG. 15 : VARIATION OF PROBE CURRENT WITH HOLE SIZE.

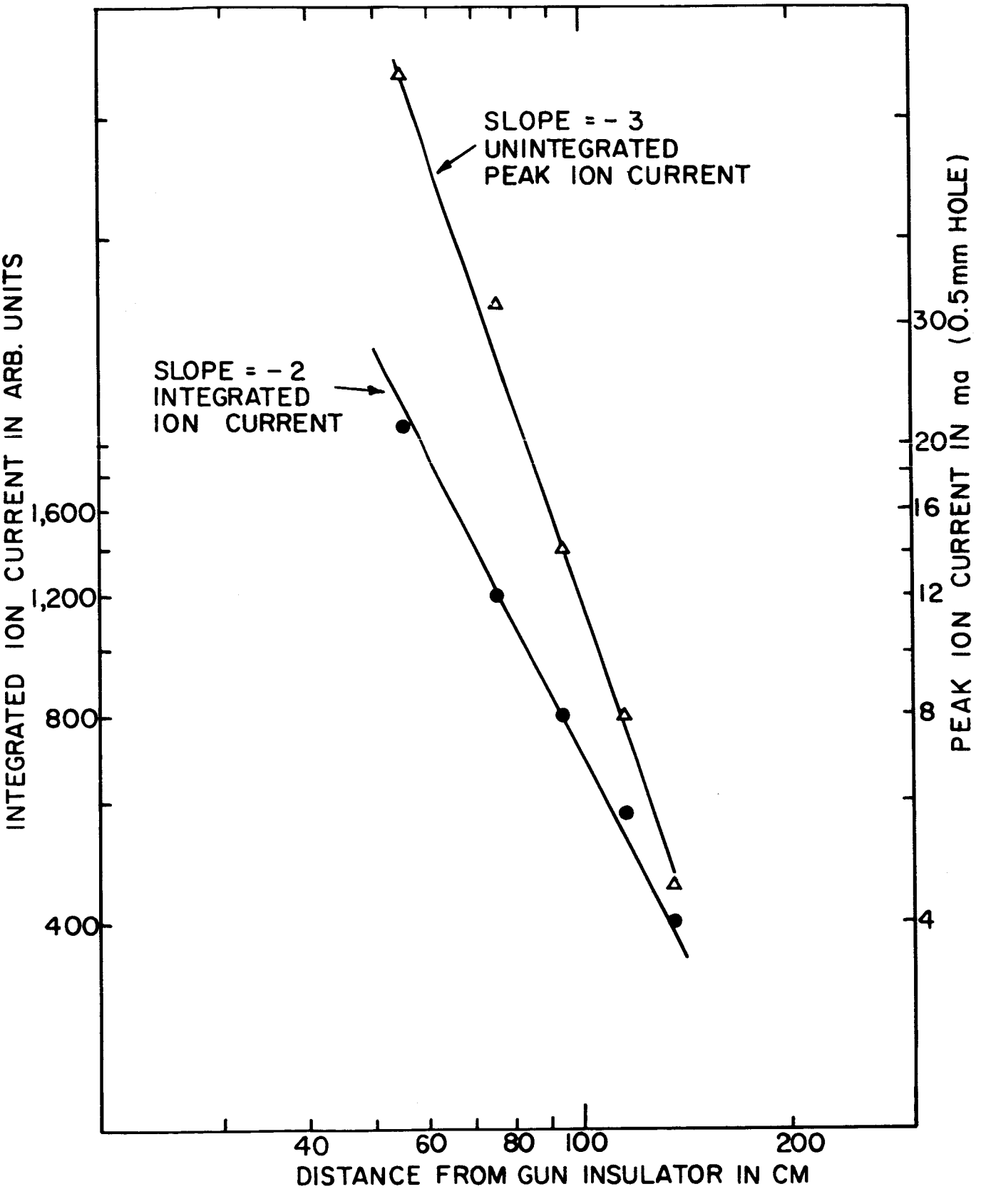

FIG. 16 : VARIATION OF PROBE CURRENT WITH DISTANCE FROM THE GUN

of firing a small signal is seen which is presumably caused by photo-electrons produced by radiation from the gun, this is easily distinguished from the main signal. Nitrogen ions at the energies used should produce insignificant yield of secondary electrons and of these the majority should not escape from within the cup.

II. 2 Electrostatic Analyzer Experiments

An electrostatic analyzer similar to that described by Eubank[12] has been used to measure the energies and the charge-to-mass ratio of ions in the exhaust. The analyzer, although it provided extremely accurate mass resolution, was not convenient for quick qualitative surveys of the exhaust products; the Faraday Cup probe described previously was convenient for this purpose, although the charge-to-mass ratio of the ions had to be assumed. For this reason the two were compared in preparation for exhaust measurements using the Faraday Cup.

We assumed that the exhaust was dominantly N^+ and obtained a velocity spectrum dn/dv with the Faraday Cup probe that was significantly different to the distribution recorded by the electrostatic analyzer. The two velocity distributions are shown in Fig. 17.

Upon investigation several inconsistencies were noticed in the electrostatic analyzer data. According to theory the velocity selected by the analyzer should vary as $\phi^{1/2}$, where ϕ is the deflector plate voltage; while the transit time spread Δt should be proportional to the transit time, t. The data shown in Figs. 18 and 19 show that neither of these conditions occur, and furthermore the ratio $\Delta t/t$ is an order of magnitude too large. However the ratio z/m of different ionic species can still be identified.

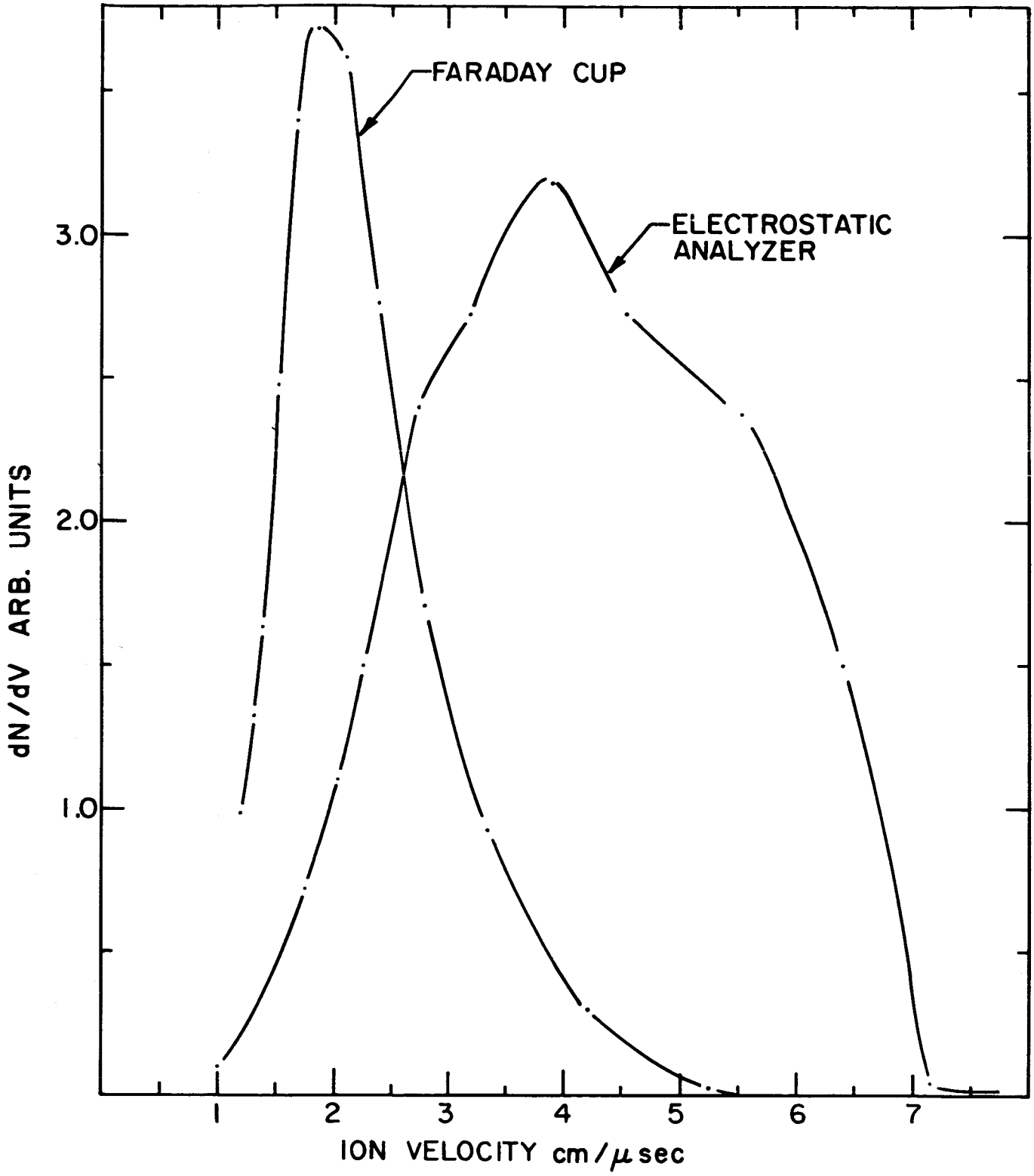

FIG. 17 : ION VELOCITY SPECTRUM

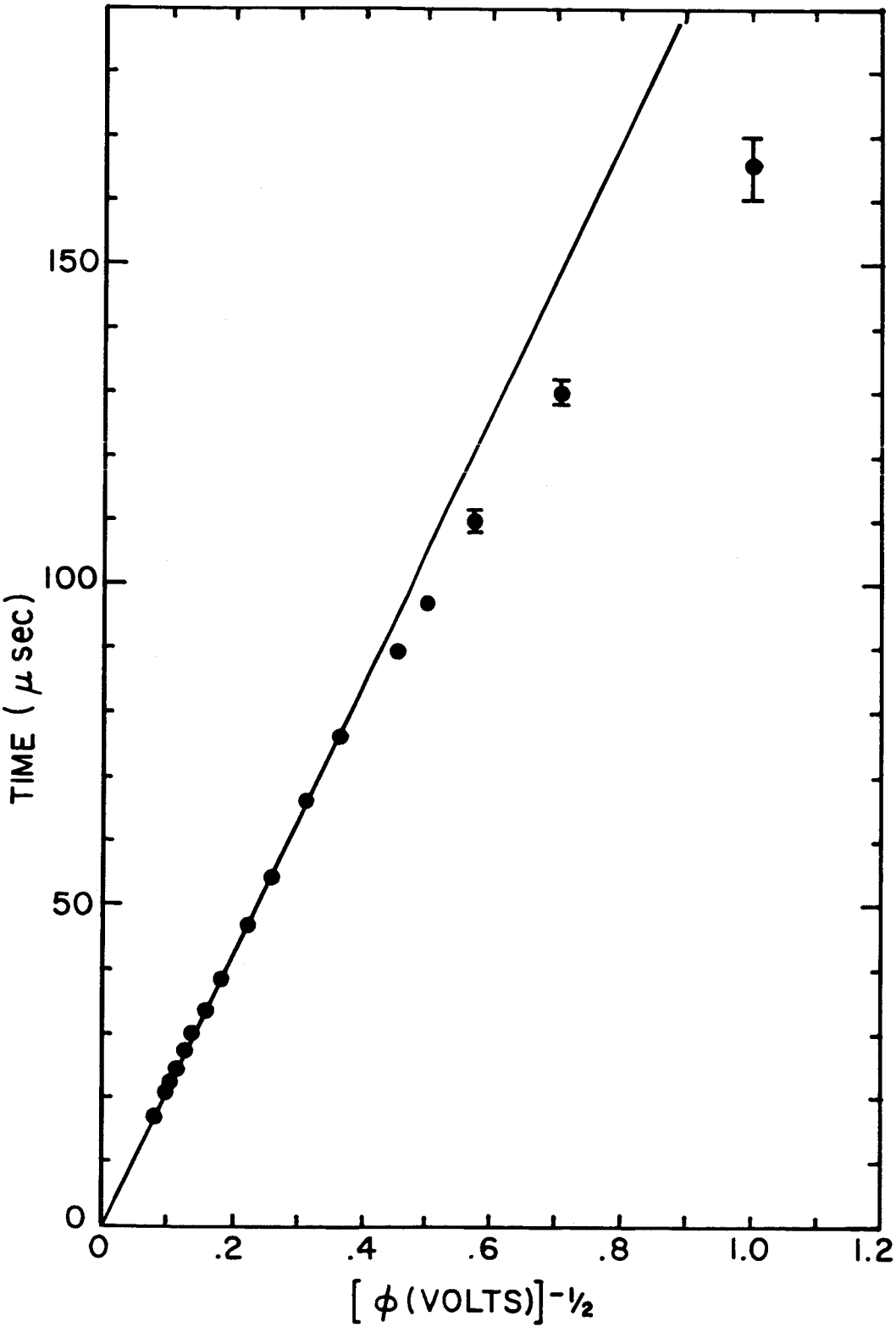

FIG. 18 : TIME OF FLIGHT VERSUS (DEFLECTOR VOLTAGE)$^{-1/2}$

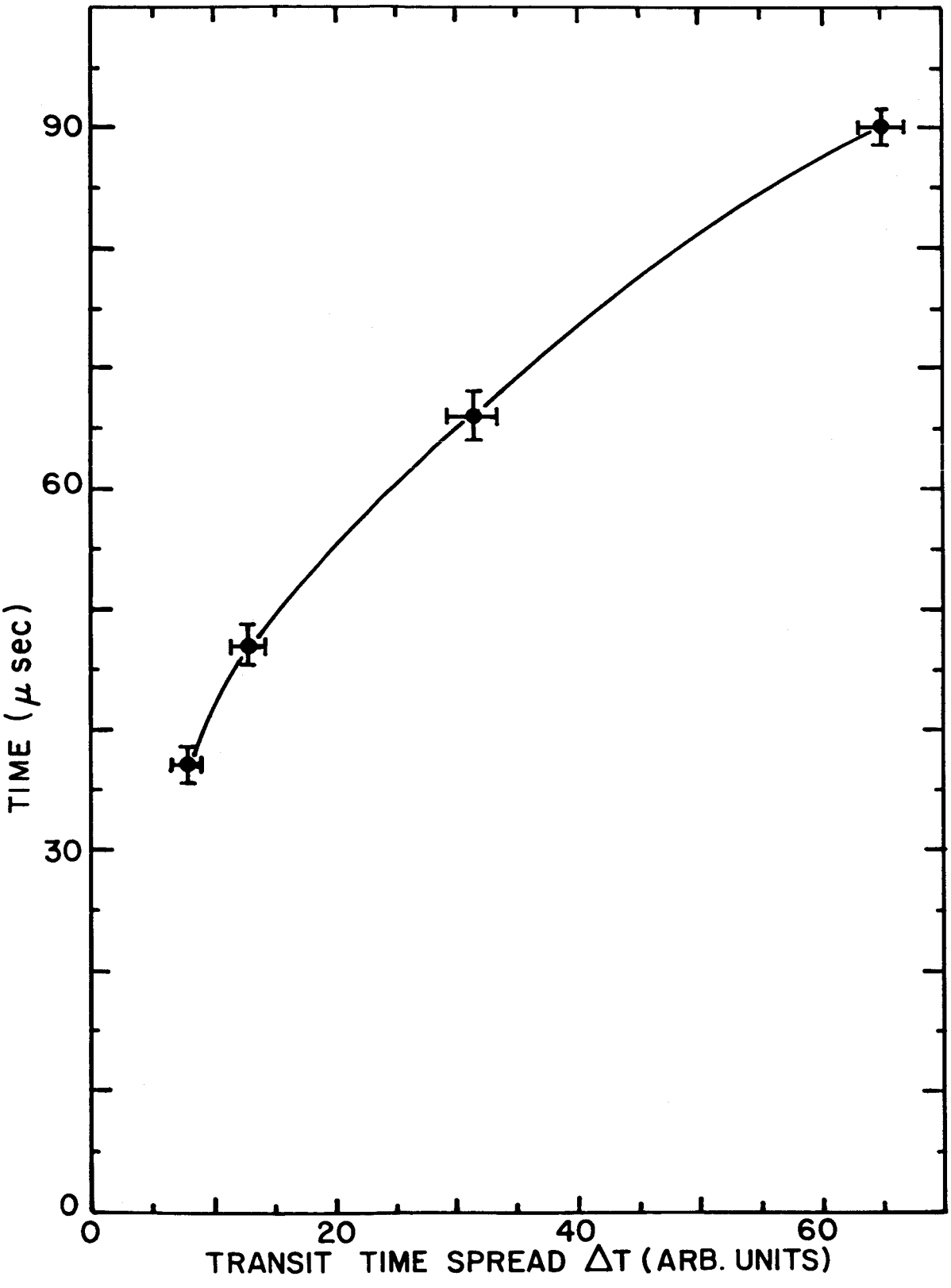

FIG. 19 : TRANSIT TIME SPREAD VERSUS TRANSIT TIME

We looked for velocity dependent collection efficiencies in the post accelerator-scintillator section by varying the post accelerator voltage and position, but found none. The entrance slit to the deflector plates had been made 3 mil; it was closed up another order of magnitude without any change in spectral shape. However, the density measured by the Faraday Cup indicates that the slit width was, and probably always has been, 3-4 orders of magnitude greater than the criterion given in the last year's final report[2] (i.e., $\phi/d \gg \frac{nex}{\epsilon_o}$). This criterion is essentially an approximate relationship between the applied electric field and the induced field due to the polarization of the beam.

Attention was also given to phenomena between the deflector plates. Once the electrons are stripped, the ion beam will expand because individual charged particles repel each other. Analysis of beam spreading[13] reveals that if

$$\frac{2\pi n_i \ell^2 e}{\epsilon_o V_i} \gg 1$$

where

n_i = ion density

ℓ = length of deflector plates (20 cm)

e = electronic charge

ϵ_o = permittivity of space

V_i = ion energy in volts

then the beam goes into a 45° spread before a significant traversal of the deflector length has occurred. To avoid this effect, n_i must be less than

10^6 cm^{-3} for 100 volt ions, the fast component of the test spectrum, and proportionately less for lesser energy ions. The density as measured by the Faraday Cup was found to be 5 orders of magnitude too large.

It is not surprising, then, to find the inconsistencies in the electrostatic analyzer data. To explain that the analyzer does report proper m/z selection and time of flight in spite of beam blow-up, one need only to realize that some particles do remain on axis. Predicting the transit time spread in the selection process is also complicated by the beam spreading effect.

The beam density was reduced to approximately 10^6 cm^{-3} by introducing additional collimators, and while the electrostatic analyzer spectrum did move to somewhat lower velocities the disagreement with the spectrum from the Faraday Cup probe was still serious. Any further reduction in density would have resulted in signal amplitude problems. Rather than confront the amplitude problems or the measurement of the ion beam trajectories within the analyzer we decided to test a Faraday Cup with biased grids. This work is in progress.

II. 3 Neutral Gas Measurements

A fast acting ionization gauge[14] has been used to measure the neutral gas distribution, at the moment of firing, both internal and external to the gun. The circuit used is shown in Fig. 20. The gauge was a 6AH6 vacuum tube with the glass envelope removed. The tube was positioned so that the neutral gas could flow into the electrode structure unimpeded by the electrodes themselves; when used inside the gun barrels the top mica supporting the anode was partially removed to improve access. The

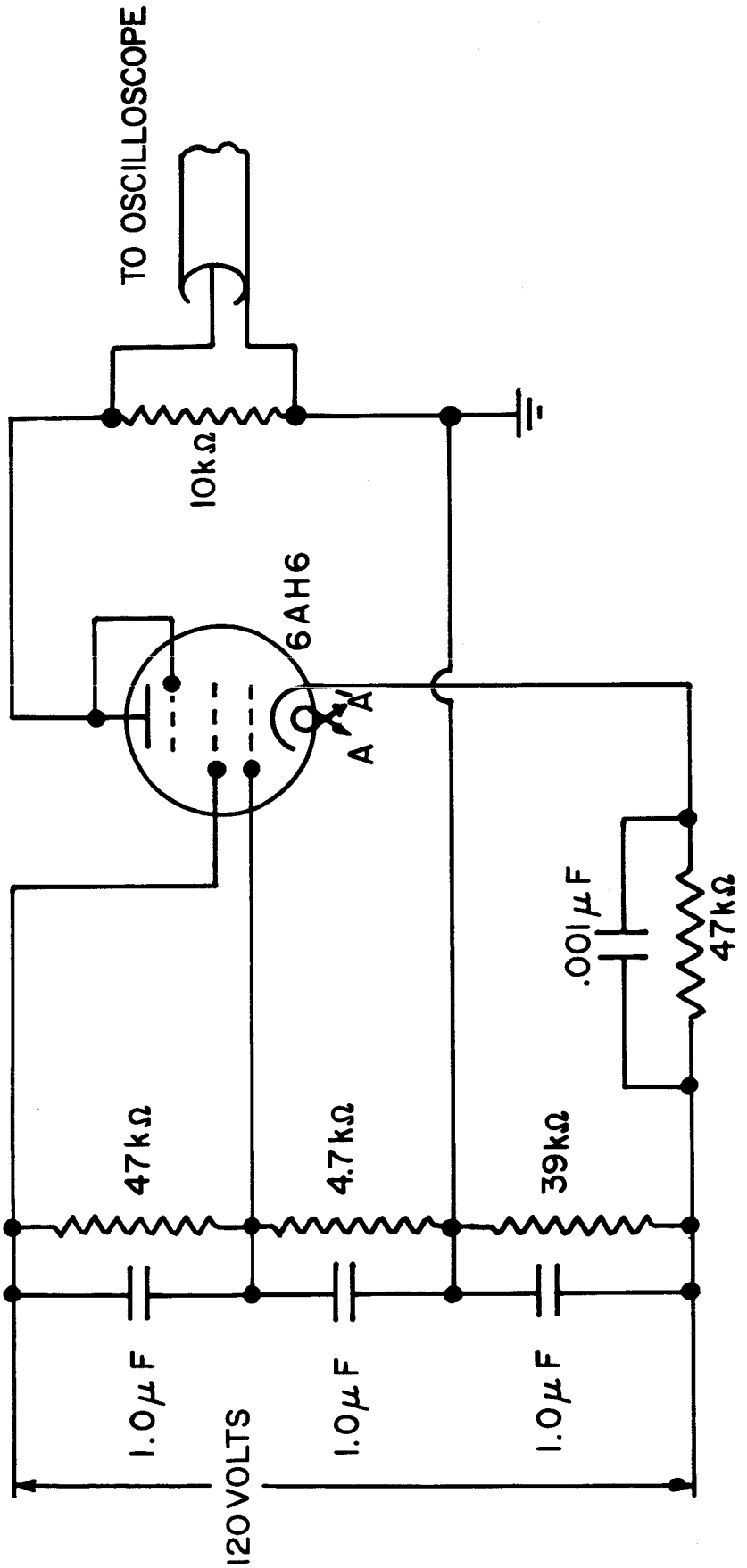

FIG. 20: FAST-ACTING IONIZATION GAUGE CIRCUIT

gauge was calibrated by pulsing gas into a closed vacuum system containing the tube and a Pirani Gauge which had been checked against a McLeod Gauge. When 120 volts was supplied to the ionization gauge circuit its response was linear with nitrogen to a pressure of 30 microns with a typical sensitivity of 10 mV/micron; by halving the applied voltage linearity was extended to 80 microns. Pressures up to 100 microns were measured by calibrating the non-linear region.

The gas distribution measurements external to the gun were made in the large vacuum tank but it was more convenient to do the internal measurements and the calibration in a smaller vacuum vessel.

Figure 21 shows the distributions of neutral nitrogen, near to the instant of firing. At this time the gas distribution is changing so rapidly that the day-to-day variation in firing time makes the actual distribution indeterminate; however, it does lie between the two extremes shown.

There are two main points of interest; firstly, the amount of gas external to the gun is small and, secondly, the number of neutral particles in the gun at the instant of firing ($\sim 2 \times 10^{18}$) is in crude agreement (a factor of two) with the number in the exhaust as determined by the ion probe.

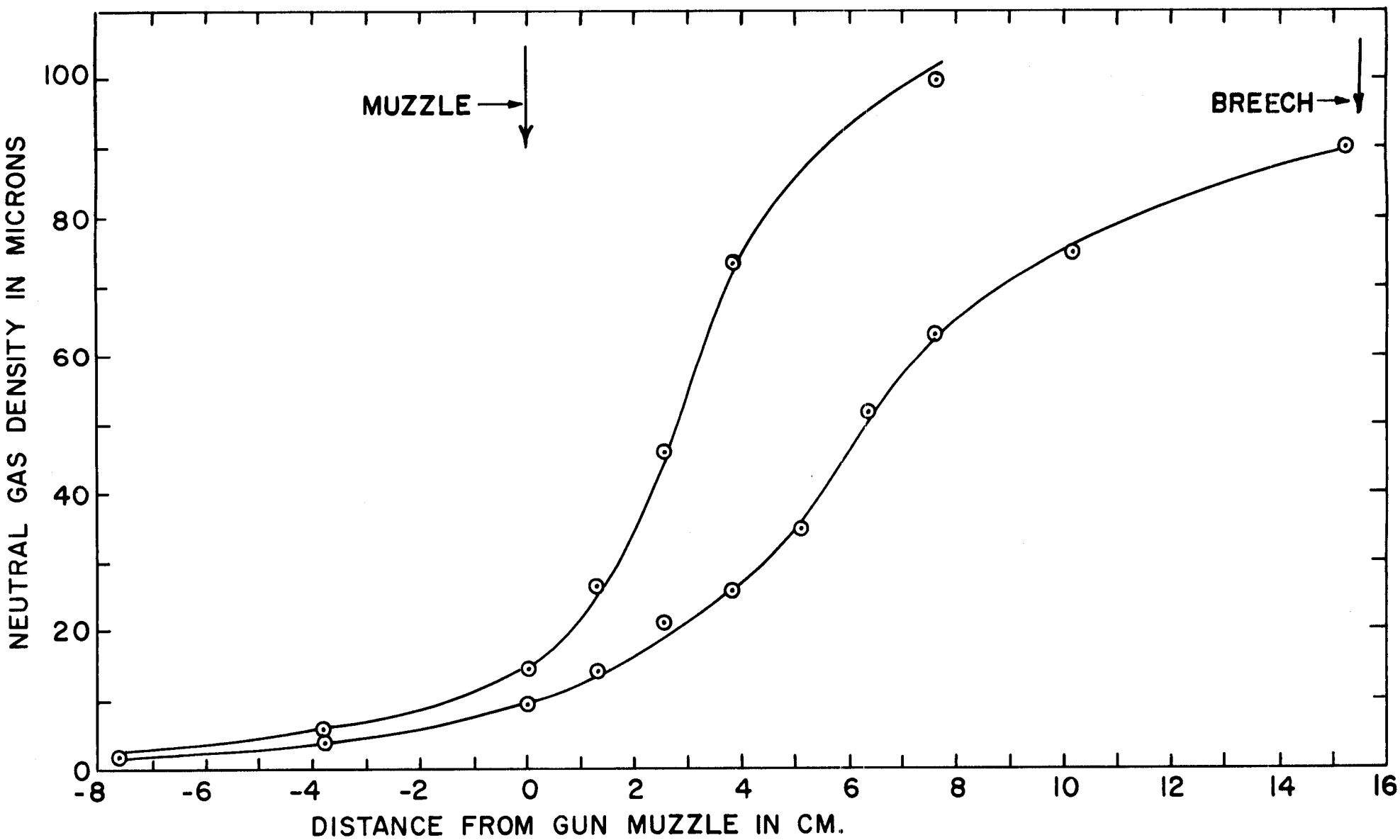

FIG. 21 : NEUTRAL GAS DENSITY DISTRIBUTIONS NEAR THE MOMENT OF FIRING

Appendix III. Pulse-Lines

The Mark IX pulse line illustrated in Figs. 3 and 4 was built because we wanted to increase the energy-storage capacitance from about 10 μfarads to 20 μfarads. It was impractical, in terms of size, weight and cost to continue paralleling small capacitors, as had been done in the earlier guns, so we decided to fabricate a single unit. It was built at GD/Astronautics because commercial manufacturers considered it neither practical, nor economical, to integrate the total required capacitance into one package. The prototype unit worked very well and we were pleasantly surprised when we obtained the waveforms shown in Fig. 9 and realized that the method of construction used in this capacitor leads to pulse-line behavior.

In a pulse-line the current amplitude and period can be controlled independently whereas in a capacitor the capacitance influences both. In plasma accelerator research it often is convenient to be able to vary peak current and period independently and to be able to tailor current and voltage waveforms for a particular application. In a final propulsion system the energy-storage element may behave like a low inductance capacitor; however, the knowledge gained and the flexibility available through the pulse-line type of construction will be invaluable.

The construction of the Mark IX capacitor is illustrated schematically in Fig. 22; it is essentially the same as the conventional extended foil construction; however, particular care is taken to avoid parasitic inductance in the connections. In the limit that the metal foils are thin compared with a skin depth the capacitor can be considered as a distributed parameter

pulse line in which the electromagnetic wave that is discharging the foils propagates radially. The direction of propagation depends on the location of the return current strap.[15]

Considering each pair of foils and insulating section as an element of the line, the distributed parameters L' and C' and the impedance Z_o and pulse time δ are given by the following equations

$$L' = \frac{\mu \ell}{2\pi} \log\left(\frac{r+d}{r}\right)$$

$$C' = 2\pi \epsilon \ell \left[\log\left(\frac{r+d}{r}\right)\right]^{-1}$$

$$Z_o(r) = \left(\frac{L'}{C'}\right)^{1/2} = \left(\frac{\mu}{\epsilon}\right)^{1/2} \frac{\log\left(\frac{r+d}{r}\right)}{2\pi}$$

$$\delta = n(L'C')^{1/2} = n\ell(\mu\epsilon)^{1/2}$$

where ℓ = width of the foil, d = thickness of the dielectric, r = the radius of the segment and n = the number of segments.

The values of Z_o and δ calculated from these formulas agree very well with the measured values. The impedance depends on radius and can be made to increase or decrease during the pulse, depending on whether the wave propagates inwards or outwards.[15]

The solutions to the circuit equations for a pulse line of constant impedance discharging into an inductive load, with an inductance given

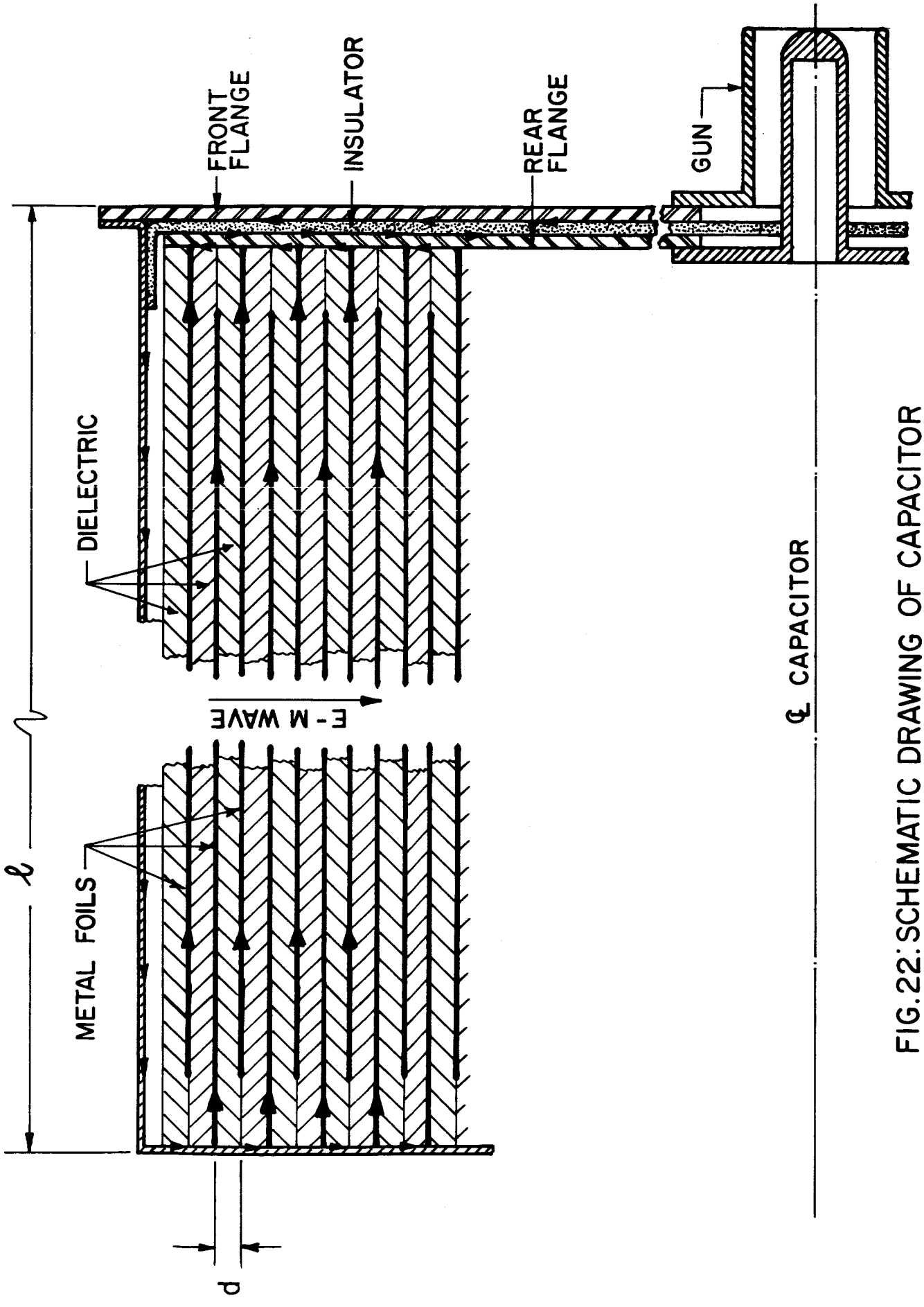

FIG. 22: SCHEMATIC DRAWING OF CAPACITOR

by $L(t) = L_o + \alpha t$, have been computed. We know that in our plasma accelerator the load closely resembles a variable inductance, with a constant α = 14 mΩ for a barrel diameter ratio of 2:1 and a sheet speed of 10 cm/μsec. The computer solutions shown in Figs. 23 and 24 illustrate the effect of varying the pulse time and impedance.

Several pulse-lines have been fabricated with various impedances and pulse-times; the objective is to develop the technology and also to investigate the performance of the accelerator for different energy-sources; work towards this aim is in progress and will be reported at a later date.

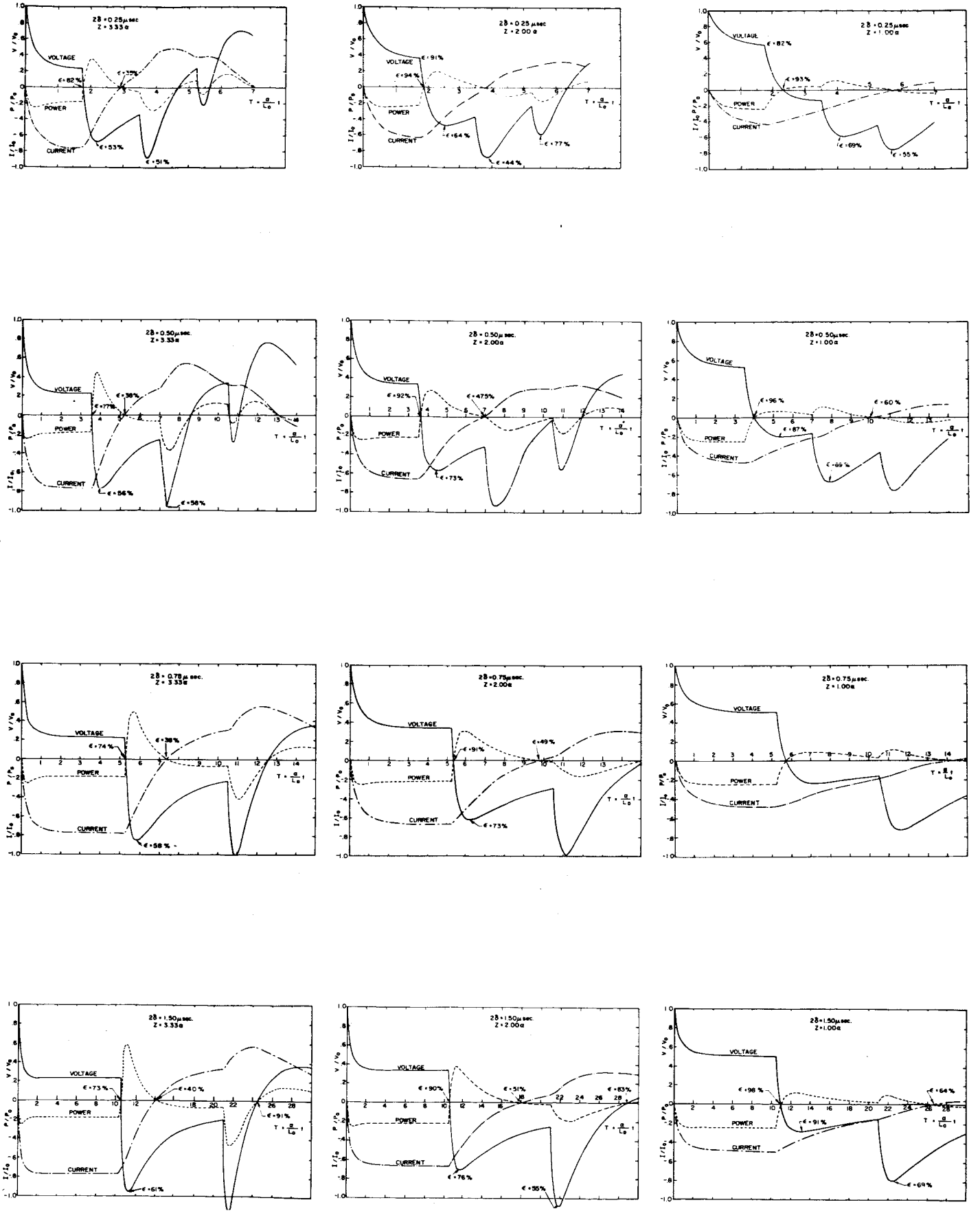

FIG. 23 : COMPUTER SOLUTIONS FOR VARIABLE INDUCTANCE LOAD, $Z_0 \geq \alpha$.

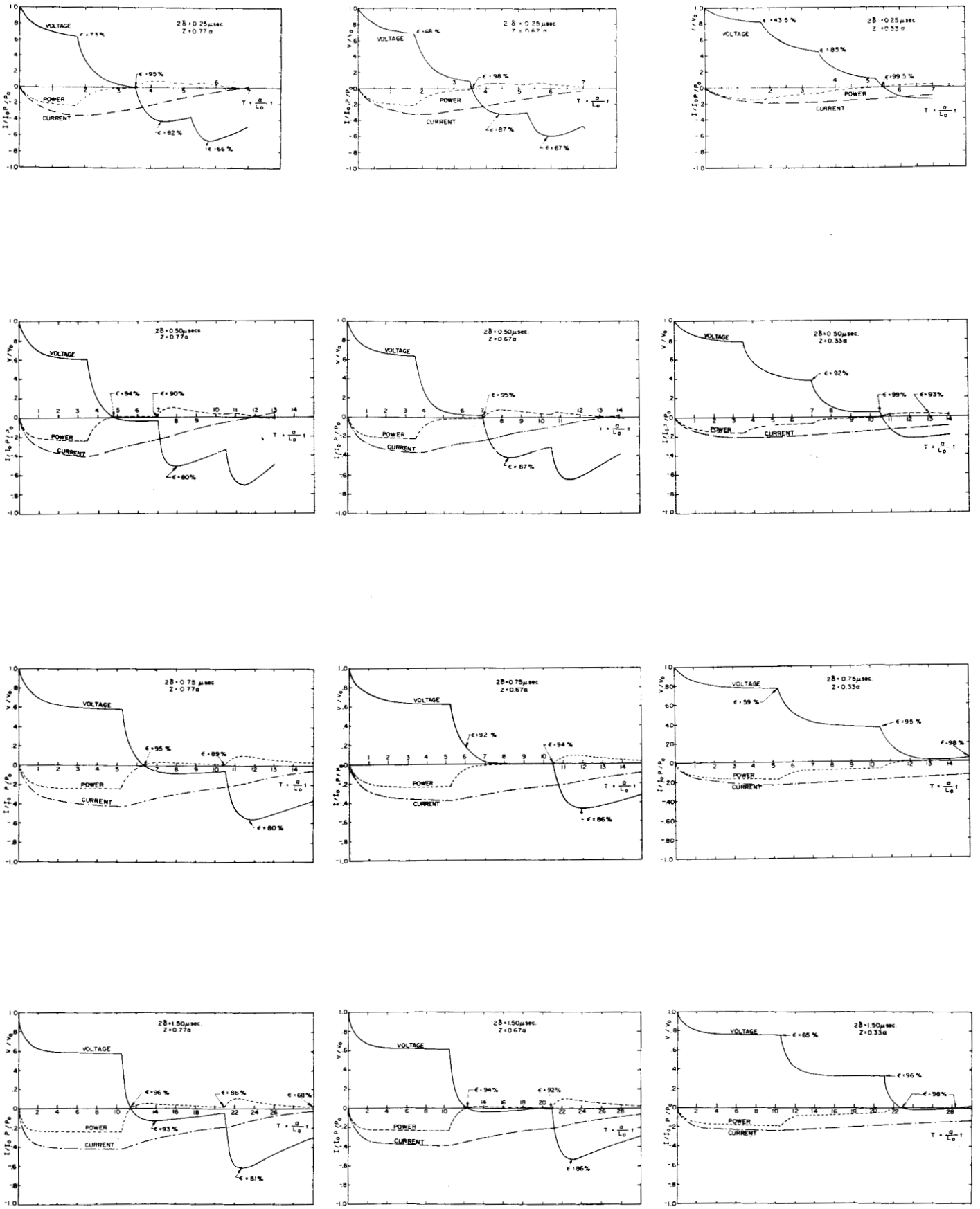

FIG. 24 : COMPUTER SOLUTIONS FOR VARIABLE INDUCTANCE LOAD, $Z_0 \leq \alpha$.

References

1. "The Use of a Co-Axial Gun for Plasma Propulsion," by R.H. Lovberg, B.R. Hayworth, T.J. Gooding, Final Report on Contract NAS5-1139, GD/Astronautics Report No. AE62-0678, May 1962.
2. "Development of a Co-Axial Gun for Space Propulsion," by T.J. Gooding, B.R. Hayworth, R.H. Lovberg, Final Report on Contract NAS3-2501, GD/Astronautics Report No. GD/A63-0454, May 1963.
3. Mostov, P. M., Neuringer, J. L., and Rigney, D. S., Phys. of Fluids, 4, 9, 1097 (1961).
4. Camac, M., Kantrowitz, A. and Petschek, H. E., I.R.E. Trans. on Military Electronics, 3, 2, 1958 (1959).
5. Hart, P. J., Phys. of Fluids, 5, 1, 38 (1962).
6. Rosenbluth, M. N., Magnetohydrodynamics, ed. by R.K.M. Landshaff, Stanford University Press, 1957.
7. Post, R. F., J. Nucl. Energy, Part C, 3, 273, (1961).
8. Kolb, A. C. and McWhirter, R.W.P., Phys. of Fluids, 7, 4, Apr. 1964.
9. Glasstone, S. and Lovberg, R. H., Controlled Thermonuclear Reactions, D. Van Nostrand, 100, (1960).
10. Coensgen, F. H. et al., Phys. of Fluids, 3, 764, (1960).
11. Ashby, D.E.T.F., Proc. VIth Int. Conf. on Ionization Phenomena in Gases, Paris, 1963.
12. Eubank, H. P., R.S.I., Vol. 34, No. 1, Jan. 1963.
13. "Fundamentals of Electronic Motion," W. Horman, McGraw-Hill, 1953, p. 152.
14. "Hydromagnetic Plasma Gun," by J. Marshall, p. 60 in "Plasma Acceleration," by Kash, Stanford University Press, 1960.
15. B. R. Hayworth, M.S. Thesis, San Diego State College, 1964.

ERRATA

NASA CR-45149

DEVELOPMENT OF A COAXIAL PLASMA GUN FOR SPACE PROPULSION

by Terence J. Gooding, Bruce R. Hayworth,
Alan V. Larson, and David E. T. F. Ashby
General Dynamics/Astronautics
San Diego, California

Cover and title page: The code number of this report, should be CR-54149 instead of CR-45149